The Thesis Committee for Anthony Ho
Certifies that this is the approved version of the following thesis:

Testing Geologic and Geometric Effects on Drilling Operations Using Torque and Drag Models

APPROVED BY
SUPERVISING COMMITTEE:

Supervisor:

K. E. Gray

Hugh Daigle

Testing Geologic and Geometric Effects on Drilling Operations Using Torque and Drag Models

by

Anthony Ho, B.S.P.E.

Thesis

Presented to the Faculty of the Graduate School of

The University of Texas at Austin

in Partial Fulfillment

of the Requirements

for the Degree of

Master of Science in Engineering

The University of Texas at Austin

December 2015

Dedication

To Furly. You are missed.

Acknowledgements

I'd like to thank Dr. Gray for not giving up on me (much) and for my family for being as patient as they are.

Abstract

Testing Geologic and Geometric Effects on Drilling Operations Using Torque and Drag Models

Anthony Ho, M.S.E.

The University of Texas at Austin, 2015

Supervisor: K. E. Gray

Intuitively, geologic and geometric effects on torque and drag should be significant. But literature suggests otherwise. Lesage et al. (1988) wrote that friction coefficients are not affected by lithology and hole angle, among other things. And if friction coefficients are similar for all of these factors, then only inclination, azimuth, and pipe specifications affect torque and drag. My thesis looks to test this statement using Johancsik's torque and drag model and data provided by our sponsors.

Johancsik's model was chosen to test these effects because it is the most widely used torque and drag model in industry. Johancsik's model also only relies on surface data in order to conduct an analysis. This contributes to the widespread use of Johancsik's model and therefore increases the applicability of this paper.

Once Johancsik's model was chosen, it became natural to choose the minimum curvature method to interpolate the wellbore trajectory because Johancsik's model was designed using the minimum-curvature method. Also, the minimum curvature method is the most widely used wellbore-interpolation method in industry. By using the minimum curvature method, this paper increases its applicability to industry.

The analyses were conducted by examining the friction coefficients of each individual formation and lithology and geometric section. Friction factors encompass all factors that are not explicitly captured by the model and any factors affecting torque and drag that are not in the model will be captured by the friction factors.

This study found lithology effects to affect drag consistently, though more data is needed. Drag friction factors were consistent by lithology, though they did appeared less predictable in Dataset 1 than the Datasets 2 and 3. Lithology affected torque less consistently than it did drag, though again more data is needed. Again, the results from Dataset 1 appeared to differ from Datasets 2 and 3. Further analyses are needed to conclude if this is caused by factors unrelated to lithology or individual geologies.

The geometric effects of curved versus straight sections appear to not affect torque and drag. The results from the curved sections from the analyses have little relation to each other. As for more specific geometries, more analyses are needed before conclusions can be reached.

Table of Contents

List of Tables

List of Figures

CHAPTER 1: INTRODUCTION

Presentation of Problem

This paper hopes to explore the effect of geology and geometry on torque and drag models. Intuitively, both should have significant effects on torque and drag calculations. Some geologic formations are harder than others and that some formations are easier to drill than others (Pessier 1994), which suggests that there will be different torque and drag effects for different formations. But some studies suggest that different geologies do not affect torque and drag in any meaningful way (Lesage 1988). Furthermore, it has been further suggested that hole angle has little effect on friction (Lesage 1988), which implies that a wellbore's trajectory has little effect on the torque and drag.

This paper hopes to determine conclusively the extent that geology and trajectory have on torque and drag calculations. Using field data provided by this project's sponsors, three analyses were conducted using common industry models. Each analysis was conducted by changes in geologic formation and again by the changes in the wellbore trajectory. Differences in the Coulomb friction factor were noted at each change. Because the Coulomb friction factor combines many unknown characteristics into a single factor, any effects on the torque and drag will be captured as changes in the friction factor. Thus, by examining changes in the friction factor alongside changes in geology and geometry, their effect on torque and drag could be analyzed.

Introduction to Torque and Drag

During the drilling process, many factors must be accounted for. The geology, the equipment, the drilling fluids, the stresses within and upon the drill string, and the wellbore geometry are a small sample of the factors that affect the drilling process during either the pre-drill planning, the actual drilling, the post-drill analysis, or a combination of multiple stages. If any of these factors is ignored, then at best the well is drilled suboptimally. The best-case scenario for such an operation is increased stress on its equipment, increased non-productive time, and a lower bottom line in its monetary returns. The worst-case scenario for such an operation, meanwhile, is a lost well that produces no monetary return at all.

One of the most important factors that must be accounted for during each stage of the drilling process is torque and drag. During the drilling process, the drill string is rotated so that the drill bit can mill away the formation and drilled to the desired target depth. But while rotating, the drill string will contact the wellbore and create a friction torque that acts counter to the direction of the drill string's rotation. This friction torque must be overcome in order to rotate the drill string. The magnitude of the torque also increases as the depth of the well increases. This makes sense—as the well is drilled deeper, there is more wellbore for the drill string to contact and more friction to overcome. Similarly, there is also an axial friction force, or drag, that acts counter to the direction of motion as the drill string is pulled out of hole (POOH) or run into hole (RIH). This force must also be overcome in order to drill.

This creates two limits that the torque applied to the drill string must be between in order to drill. The lower limit is the friction discussed above. The upper limit is the physical limit that the drill string can handle without being damaged. If the applied torque exceeds the maximum torque specified by the drill pipe, it can result in a deformed or damaged drill string. In extreme cases, too much torque can cause drill pipe can become disconnected from each other, a phenomenon known as "twist off" (Johnson 2010). It is therefore imperative that the applied torque be less than maximum torque allowed by the pipe specifications.

Thus, in the pre-drill planning stage of the drilling process, the wellbore must be designed so that the expected amount of applied torque never exceeds the drill pipe's maximum allowable torque specifications yet is larger than the friction. This creates limits for a number of facets in the wellbore design. Most noticeably, the maximum torque limits how far the target depth can be set. As the depth increases, the frictional torque acting on the drill string increases. At some depth, the frictional torque will equal the maximum allowable torque on the drill string. At this point, the torque required to rotate the drillstring will result in drill string failure. Banks et al. (1992) and Payne and Abbassian (1997) discuss the idea of designing a well plan that limits the torque on the drill string in order to reach a greater target depth. Sheppard et al. (1987) also discuss planning a wellbore in order to reduce the torque on the drill string. If the expected torque continues to exceed the drill pipe specifications despite choosing an efficient geometry, then other torque reduction measures such as tool-joint stress balancing and high-friction

thread compounds (Payne 1997) should be used. Ho (1988) mentions that torque should be a consideration for a "more realistic drill string design and surface equipment selection."

Torque is also an important factor while drilling. In addition to being a limiting factor that should not exceed the pipe specifications, torque can be used as a means to detect cuttings buildup. A sudden rise in the torque or drag measurements while drilling can be a sign that cuttings are building up and preventing the drill string from rotating efficiently. This phenomenon is discussed by Kucs (2008) and implied by McCormick and Liu (2012). Similarly, torque can also be used to detect differential sticking while drilling. Differential sticking occurs when the drill string becomes stuck to the wellbore and fails to rotate downhole. The top of drill string continues to rotate, however, building up tension along the drill string. Eventually this tension will release the drill string, causing it to rotate very quickly as the built up tension is released. The signs of differential sticking is an increase in the drill string torque and a simultaneous drop in revolutions per minute (RPM), followed by a sudden drop in torque and a large increase in RPM. Differential sticking is a drilling hazard because it leads to increased strain on the equipment and drill string. But by accounting for the torque and RPM, differential sticking can be avoided during the drilling process (Brett 1989). Kucs (2008) describe a method to detect differential sticking by examining the drag forces. This method examines the out of slip weights and compares it to the expected hook load value based on the number of stands drilled. If the out-of-slip weight is much lower than the expected

hook load, then some of the weight is being borne by the drill string being stuck to the wellbore. In a similar manner, torque can be used as a measure to optimize the drilling procedure. Rae et al. (2005) claimed that excessive drag forces can be resolved by applying more weight-on-bit (WOB). This forces the drilling process to overcome the drag forces. Similar issues can be identified early by examining torque and drag and countermeasures can be taken to resolve these issues.

Torque and drag are also key factors in the post-drill analysis. If a well failed to reach its target depth, torque and drag the torque and drag logs can be examined to identify what issues were experienced during the drilling operation. Brett (1989) wrote, "…torque and drag data collected while a well is drilled… can be used to evaluate why the well did not reach predetermined objectives." A sudden spike in torque or drag can be a sign that the well had hole cleaning issues or differential sticking. And once the proper issue is identified, proper remedial actions can be taken. If there are hole-cleaning issues, then a heavier mud can be used. If the well is experiencing differential sticking, then perhaps a new casing program should be evaluated.

It can therefore be seen that torque and drag play a vital role throughout the entire drilling process. The issue, however, is accurately predicting how much torque will be applied to the drill string during the drilling process. Torque can be readily measured at the rig site, but measuring the friction losses downhole is much more complicated. In recent years, these friction losses were measured using measurement-while-drilling (MWD) tools. MWD tools were designed to take measurements just above the drill bit

and should, in theory, provide the most accurate torque and drag measurements. In practice, however, the harsh downhole conditions can make downhole tools unreliable. This, along with its high costs has led industry to look at other alternatives.

One alternative that industry has explored in recent years is torque and drag modeling. Torque and drag modeling represents a cost-efficient means to estimate downhole friction losses. Whereas MWD requires specialized tools, personnel, and training, torque and drag models only require access to data that is already collected standard during drilling operations and a means to process this data (typically a program installed on a laptop). The data is fed into the laptop and processed using the program, and the end result is an estimation of the friction losses.

The issue, however, is developing an accurate torque and drag model that combines the appropriate physics and the appropriate data. There are many factors that affect friction losses, such as drilling fluids and which drill pipe is used. But there are just as many factors that have no effect on friction losses at all. Knowing which factors are important and which are extraneous are crucial to developing a working torque and drag model.

This thesis examines two factors in particular—formation geology and wellbore geometry—to explore their effect on friction losses. Intuitively, both of these should affect how much friction losses occur during drilling operations. Because different lithologies have different physical properties, it should be expected that drilling different lithologies would have different friction factors. And because of the complex nature of

drilling a horizontal well, it should be expected that friction factors would account for these complexities and be inconsistent from vertical drilling operations. Issues such as hole cleaning become a major issue during horizontal drilling operations, and it would be expected that the friction factor would represent this. But literature suggests that neither accounts for much additional friction loss. Lesage et al. (1988) suggests that friction factors are indifferent towards lithology and hole angle, among other things.

That is the purpose of this thesis—to explore the effect of geology and geometry on torque and drag models using field data provided by Wider Window sponsors. Using Johancsik's soft-string model, field data from different lithologies and different wellbore geometries were analyzed to find if friction factors are indifferent to geology and geometry.

Chapter 2 of this thesis provides background on torque and drag modeling, including various different torque and drag models used in industry. Chapter 3 describes the torque and drag model used in the analyses presented in this paper, and then details the three case studies conducted for this paper. Chapter 4 discusses the conclusions reached by this study and Chapter 5 proposes future research to be conducted in torque and drag modeling.

CHAPTER 2

Torque and Drag Model Overview

As discussed above, torque and drag models attempt to estimate the friction losses that occur during drilling operations. They analyze a variety of inputs, including drill pipe properties, wellbore geometry, and fluid properties, and estimate the magnitude of the normal force acting between the drill string and well bore. The normal force is then used to estimate the magnitude of the friction losses. Most torque and drag models use a finite element method of analysis—this is done to simplify more complex wellbore geometries. Such models divide the drill string into a number of segments and examine the forces acting on an individual drill string segment. A free body diagram of a segment can be seen in Figure 1 below.

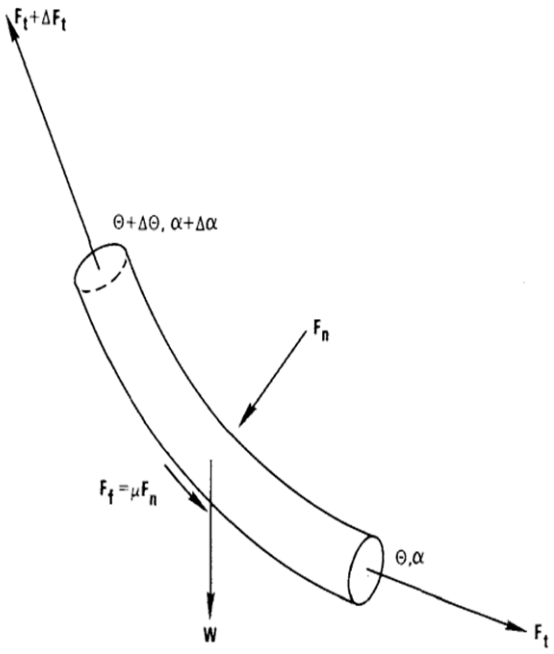

Figure 1: Free Body Diagram of Drill String Segment (Johancsik 1984)

where, in the above figure,

F_n = normal force
F_t = drill string tension
ΔF_t = change in drill string tension along drill string element
Θ = inclination
$\Delta\Theta$ = change in inclination along drill string element
α = azimuth
$\Delta\alpha$ = change in azimuth along drill string element
W = buoyed weight of drill string element
F_f = friction force
μ = coefficient of friction

The forces for all segments are then summed together. This is the total force acting upon the drill string that is used to estimates the friction losses experienced during drilling operations.

Wellbore Geometry Interpretation

In order to conduct a finite element analysis, the wellbore trajectory must be known. The properties of the wellbore trajectory, however, are only known at certain points when a directional survey is taken. During a directional survey, a well's compass coordinates, total vertical depth (TVD), inclination, and azimuth are measured. These surveys typically happen after every three stands of drill pipe, or 90 feet, have been drilled. An example well, created using fictitious data, of the "known" information can be seen in Figure 2 below.

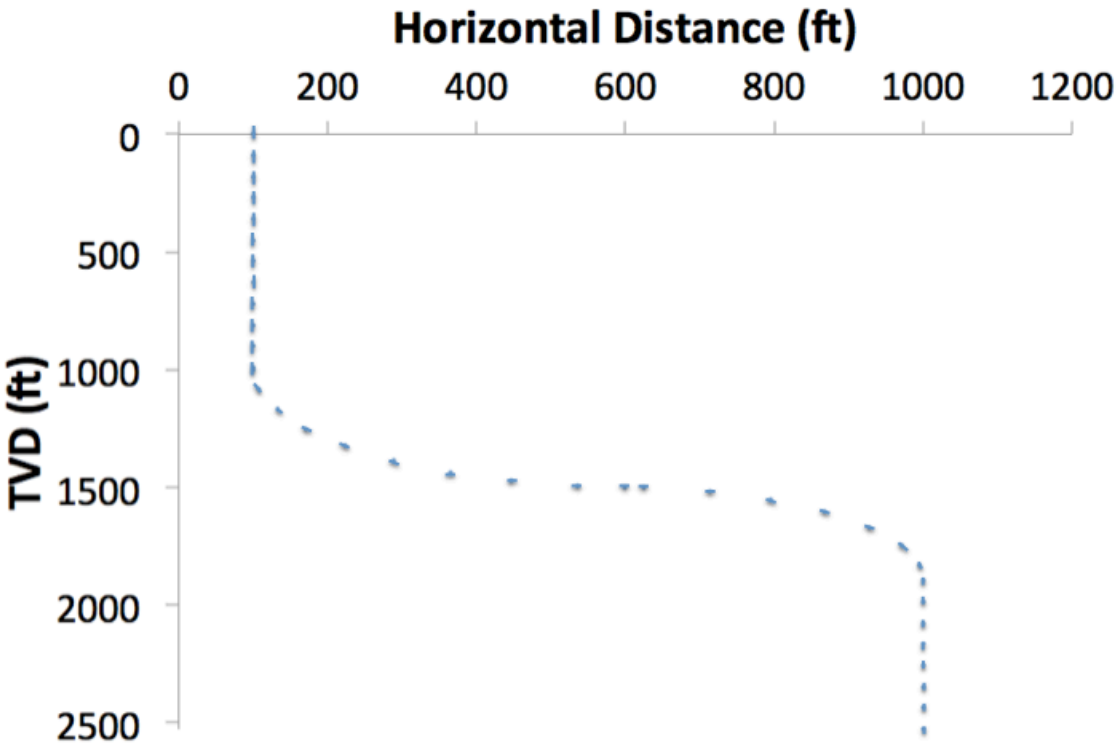

Figure 2: Sample Well of Known Information at Survey Points

In Figure 2, each dash represents the location of each survey point, while the angle of each dash represents the angle of the well's inclination. It can be seen that the trajectory between survey points is unknown and must be interpolated. There are many different possible methods that can be used to determine the wellbore's curvature. These methods include modeling a wellbore's curve as a linear line (tangential model), as the smallest possible arc that can fit between the two points (minimum curvature model), or a variety of more complex methods of interpolation (Mitchell 2008).

The simplest method of interpolation is the tangential model, which assumes that a wellbore is perfectly linear between survey points. Rather than attempt to design a smooth wellbore trajectory, this method uses the shortest distance between survey points

to design the trajectory. This method is quick and easy to calculate and, by definition, uses the least drill pipe to reach the target points. This method's angular designs, however, would result in large amounts of torque and drag on the drill string. It is thus an inefficient design and not used in industry.

The most commonly used interpolation method within industry is the minimum curvature method. This method assumes that survey points are connected by the smallest circular curve segment possible. This is a relatively simple method that has resulted in accurate torque and drag calculations and whose smoothness provides a more realistic interpretation of the wellbore geometry than the previous interpolation model. It has been suggested that more efficient trajectories exist (Sheppard 1987), but nevertheless, the minimum curvature method's ease of use and successful pedigree has made it the industry standard.

Another method is to model the well using catenary interpolation. This method models the well as a free-hanging chain suspended at the ends. It has been suggested that the calculated friction losses for this interpolation method are less than the calculated losses modeled using the minimum curvature method (Sheppard 1987). But because drilling a catenary well is much more difficult than drilling a minimum curvature well, very few wells are planned and very few torque and drag calculations made using catenary interpolation.

Mitchell and Samuel (2009) disagreed with using the minimum curvature method to model wellbore trajectory. They felt that doing so did not accurately portray the

physics acting upon the drill string. The minimum curvature method assumes the trajectory between survey points is circular and therefore has a constant curvature. At each survey point, however, the curvature jumps dramatically from one value to another. And because the bending moment is directly proportional to the curvature, the bending moment will also jump dramatically at survey points. This, Mitchell and Samuel argued, was an invalid assumption. They argued that the bending moment along a drill string should be fluid and that erratic bending moments were unrealistic. They proposed using a trajectory model that allows for a variable curvature between survey points. This would allow the bending moment to transition smoothly at survey points.

Mitchell headed the development of two such models. The first method used cubic splines to model the wellbore trajectory (Mitchell 2008). The goal of cubic spline modeling is "get an interpolation formula that is smooth in the first derivative, and continuous in the second derivative, both within an interval and at its boundaries," (Press et al. 1992). Cubic spline modeling interpolates between data points using a cubic polynomial with constant coefficients. This creates a smooth interpretation of the wellbore while also allowing smooth transitions in the bending moment. And this, Mitchell argued, created a more realistic wellbore interpolation.

Mitchell's second method assumed that the wellbore trajectory could be mapped using the minimum curvature method at specific points while the trajectory between those points were calculated using a combination of both an analytical solution (using the balance of moment on the frozen points) and a numerical solution for the continuity of

bending moment (Mitchell 2013). An example of the trajectory can be seen in Figure 3 below.

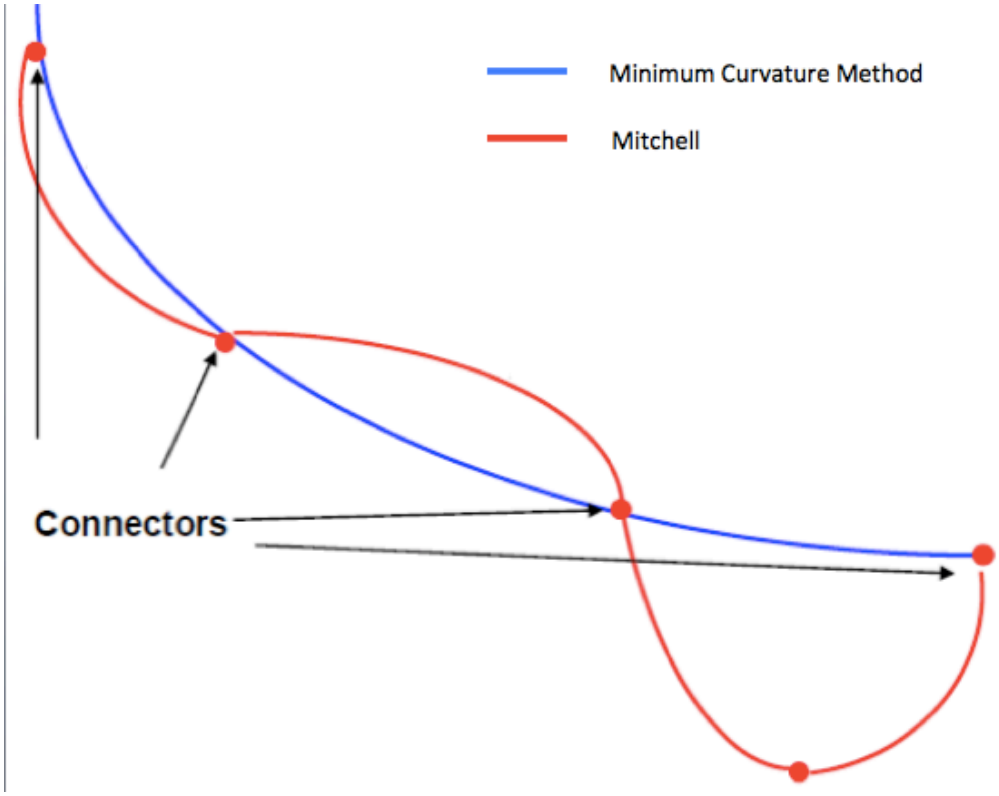

Figure 3: Assuming Wellbore Trajectory Equals Minimum Curvature as Specific Points (Mitchell 2013)

As can be seen in Figure 3, the wellbore trajectory follows the minimum curvature method only at specific points. In between these points, both analytic and numerical solutions were used to determine the well bore trajectory. The advantages of this method are that it can model point contact between the wellbore and the drill string. Other models assume there is continuous contact between the wellbore and drill string by averaging the friction losses throughout the length of the entire drill string. In these models, each increment of pipe adds a proportional amount of friction losses. The second

method, however, allows for point contact. This allows for different parts of the drill string to experience more friction than others. The principle disadvantages of this method are rooted in its complexity. 6 distinct equations and 8 distinct unknowns describe each drill string segment. A combination of analytical and numerical solutions must be used. Proper boundary conditions must be assessed before a solution can be estimated. These issues, along with the method's novelty, are the reasons why this this method is not widely used in industry.

Torque and Drag Models from Literature

Torque and drag models are generally divided into two schools—"soft-string" models and "stiff-string" models. Soft-string models are simpler than stiff-string models and assume that the bending stiffness contribution to the normal force is negligible. They also tend to assume that the drill string is completely confined by the wellbore. In other words, soft-string models assume that there is zero clearance between the wellbore and drill string, that the center of the wellbore and drill string are the same, that the trajectory of the drill string and wellbore are the same, and that the contact between the drill string and wellbore is continuous (Ho 1988). These assumptions make the calculations easier and often greatly reduce computation time (Mitchell 2013).

Stiff-string models, meanwhile, tend to be more generalized. They account for the bending stiffness contribution and do not assume that the drill string radius is equal to the wellbore radius constrained by the wellbore (Mitchell 2009). In theory, by making the model more generalized, it becomes more accurate. The downside to this, however, is

that calculations become much more complicated. The models can no longer be solved analytically and must be solved numerically. This can increase the execution times of stiff-string models to take 100 times longer than the execution time of soft-string models (Mitchell 2013). There is also no guarantee that the additional accuracy provides any benefit to the user.

JOHANCSIK'S MODEL

Johancsik's soft-string model (1984) is the most widely used torque and drag model in industry today (Mitchell 2009). It was the first torque and drag model to estimate friction losses using a finite element method to simplify the wellbore trajectory. This model divides the drill string into elements composed of circular arcs and examines the basic forces acting upon each element. It then estimates the friction losses using a lumped Coulomb friction parameter. This lumped parameter accounts for all friction losses acing upon the drill string. law to determine the change in the tension and torque along that element (see **Figure 4** below).

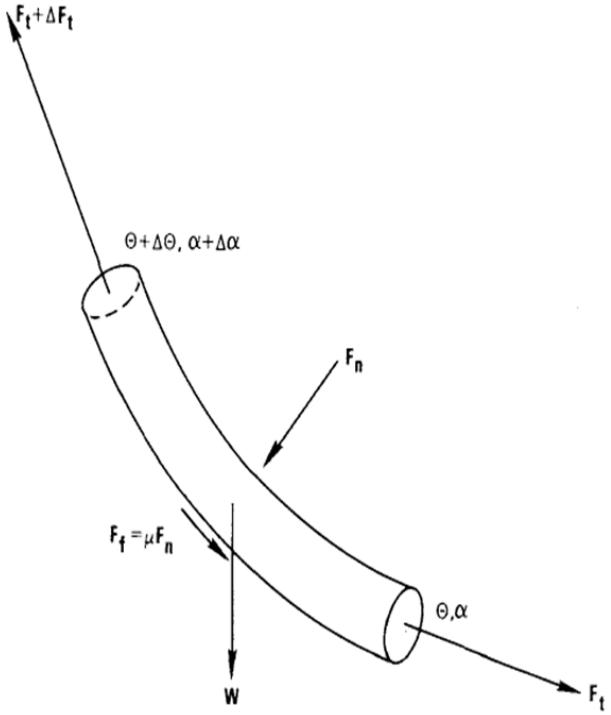

Figure 4: Forces Acting upon Drill string Element (Johancsik 1984)

where, in the above figure,

F_n = normal force
F_t = drill string tension
ΔF_t = change in drill string tension along drill string element
Θ = inclination
$\Delta\Theta$ = change in inclination along drill string element
α = azimuth
$\Delta\alpha$ = change in azimuth along drill string element
W = buoyed weight of drill string element
F_f = friction force
μ = coefficient of friction

This model assumes each drill string element has a constant curvature (using the minimum curvature method described above) as well as continuous contact between the drill string and the wellbore. The model also assumes that pipe bending contribution to the normal force is small enough to neglect.

AADNOY'S MODEL

Aadnoy (2008) expanded upon Johancsik's model to account for more complex well geometries by integrating the force balance acting on a drill string element. His derivations resulted in equations that accounted for several different wellbore geometries. These geometries are shown in **Figure 5** below.

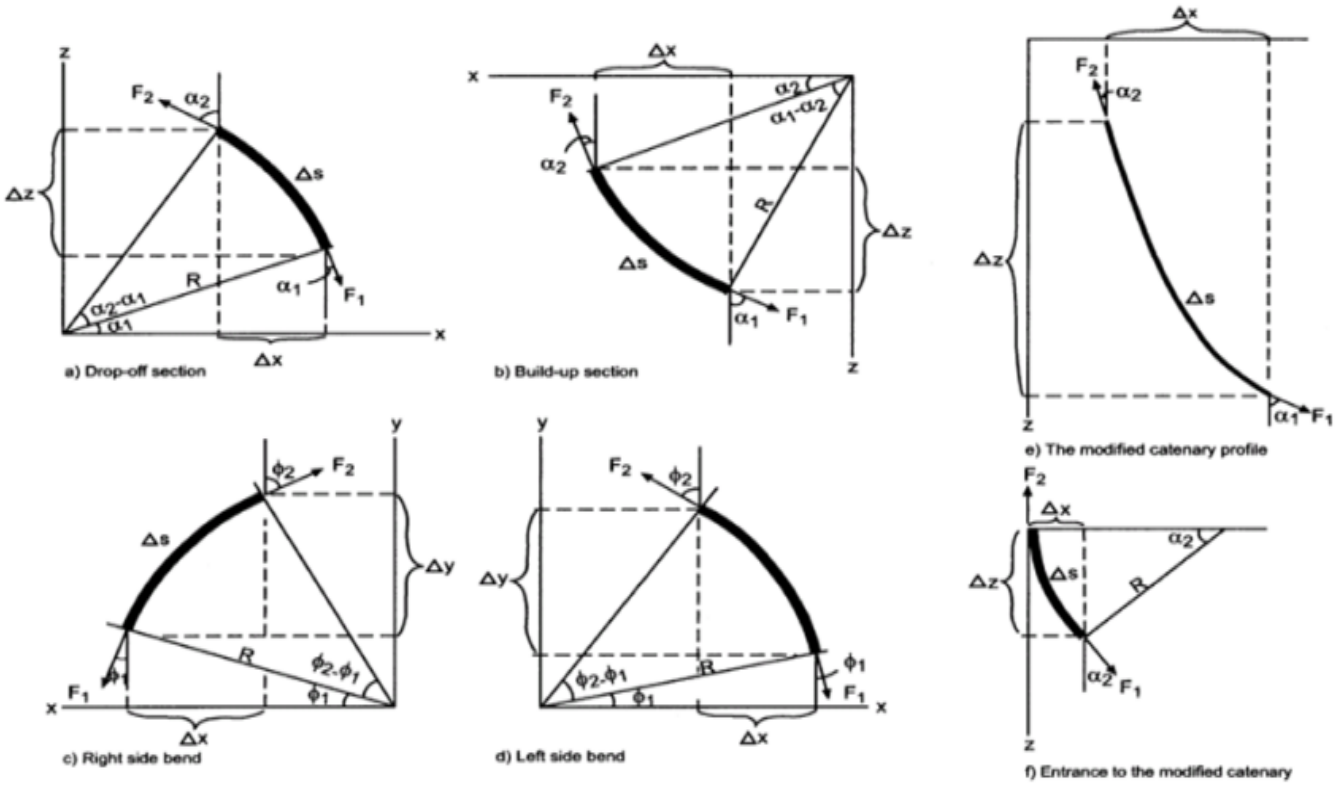

Figure 5: Wellbore Geometries Described by Aadnoy's model (1998)

where, in the above figure,

F_1 = lower drill string tension
F_2 = upper drill string tension
Δs = length of drill string element
ϕ_1 = lower azimuth
ϕ_2 = upper azimuth
R = radius of curvature

Unlike Johancsik's model, Aadnoy does not assume a constant curvature between survey points. His model is for a more general wellbore trajectory, though he also modeled the solution to a catenary well trajectory (discussed above). Finally, Aadnoy's model is also a soft-string model and assumes that the bending stiffness contributes negligibly to the normal force.

HO'S MODEL

Ho disagreed with many of the assumptions made by Johancsik and Aadnoy (Ho 1988). In particular, he disagreed that the bending stiffness was negligible. He proved the invalidity of ignoring the bending stiffness through a rigorous derivation of the tension in the drill string that demonstrated that the bending moment that runs tangential to the drill string contributes to the resultant force. The difference between a soft-string model and Ho's stiff-string model can be best demonstrated in **Figures 6 and 7** below.

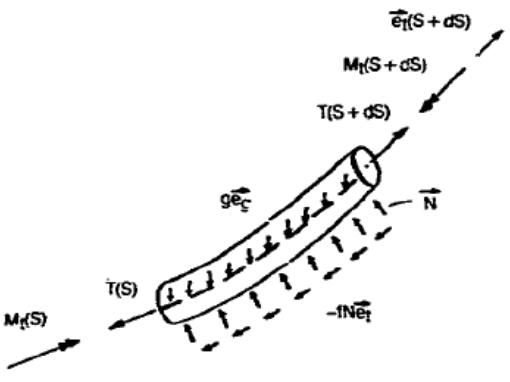

Figure 6: Soft-string Model Force Balance (Ho 1988)

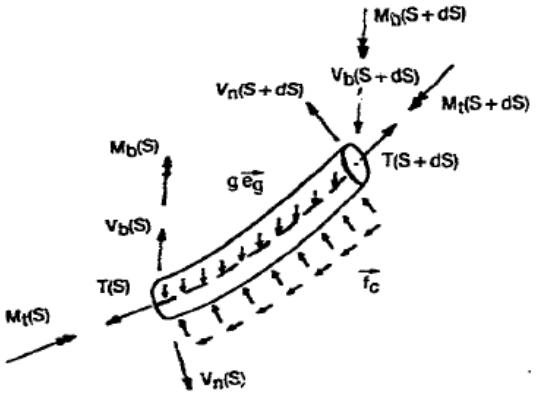

Figure 7: Stiff-string Model Force Balance (Ho 1988)

where, in the above figures,

$T(S)$ = lower drill string tension
$T(S + dS)$ = upper drill string tension
N = normal force
$M_t(S)$ = lower drill string torque
$M_t(S + \Delta S)$ = upper drill string torque
$M_b(S)$ = lower bending moment
$M_b(S + \Delta S)$ = upper bending moment
f = friction coefficient
g = submerged drill string weight per unit length
V = physical component of resultant force

In **Figures 6** and **7**, it is easy to note the bending moments (denoted by the $\vec{M}(S)$ and $\vec{V}(S)$ terms) in the stiff-string model and their absence in the soft-string model. Whereas Johancsik and Aadnoy argued that these provided negligible contributions to the normal forces, Ho argued that an accurate model needed to include these terms. These terms become especially apparent when the borehole diameter decreases. Because soft-string models assume a continuous contact between the wellbore and the drill string, the models neglect changes in the borehole diameter. Thus the effect of decreased boreholes is ignored in soft-string models. Ho's stiff-string model, however, showed a noticeable uptick in the drill string tension when the borehole diameter decreased. This is due to the bending moment contributing more tension in the drill string.

Ho's results suggest that his model is more suitable to estimate downhole torque and drag than soft-string models. Despite this, his model is less widely used than similar soft-string models. There are reasons for this. Most importantly, his model requires an estimation of the bending moments within the drill string. These values are difficult to

obtain during a drilling operation. As such, his model is difficult to run. Along similar lines, other authors have not corroborated his results. Other authors have not confirmed that the increased theoretical accuracy of Ho's model translates to better results during field operations. As such, it has been difficult for Ho's model to gain widespread use.

CHAPTER 3: ANALYSES

As stated at the beginning of this thesis, the purpose of this study was to determine the effect of geology and geometry on friction losses. This was done by analyzing the friction coefficient of three sets of field data provided by this project's sponsors. Each dataset contained the geologic information, the wellbore trajectory, and the relevant surface and downhole data necessary to estimate downhole friction losses.

Each dataset was analyzed twice for a total of six analyses in all, first by its geologic information and then again, in a separate analysis, by its wellbore trajectory. To conduct each analysis, the wells were first divided by their geologic information and by wellbore trajectories. The friction factors for each division were then estimated using a torque and drag model. The results were then compared to each other and differences in the friction factors were noted. Friction factors combine all parameters that are not expressed by the model into a single coefficient that "represents the average conditions of a particular wellbore," (Johancsik 1984). Any factors not explicitly captured in a torque and drag model is captured in the friction factor. Thus any additional geologic or geometric effect that is not explicitly modeled will be identified by changes in the friction factor.

These analyses were conducted using Johancsik's model to estimate friction losses and the minimum curvature method to estimate the wellbore trajectory. Details and equations for each method can be found in Appendix A and B, respectively. There were several reasons these methods were chosen. First, both models are the most commonly

used models in their respective fields and any analyses conducted with these models are more applicable in industry than other analyses would be. A second reason Johancsik's model was chosen was because it can be run using data that is already commonly collected, namely surface drilling data and survey data. This makes it ideal to be used in most drilling operations as no new equipment or measurements are required. And finally, Johancsik's model was used because it uses the friction parameter described above. An explanation of the how this friction parameter is calculated is given in Appendix C. The friction parameter makes identifying the effects that geology and wellbore trajectory have relatively simple, as any changes experienced during drilling operations that are not accounted for in Johancsik's model will be accounted for in the friction factor. Any geologic or geometric factors that Johancsik's model does not account for will be reflected in changes in the friction factor.

In the following sections are the detailed analyses of each dataset. Each dataset describes a drilling operation conducted by one of this project's sponsors. Each section will first give a brief description of the well and data, followed by the geologic analysis of the data, and end with the geometric analysis of the data. The accuracy of each analysis is measured by comparing the model measurements to the downhole measurements. The average difference between the surface and downhole measurements was taken as well as the average difference relative to the measurement. The average absolute difference is given by Equation 1 below, while the average relative difference is given by Equation 2 below.

Equation 1. $$\mu_{abs} = \frac{\sum_{i=1}^{n} |y_i - x_i|}{n}$$

Equation 2. $$\mu_{rel} = \frac{\sum_{i=1}^{n} \frac{|y_i - x_i|}{y_i}}{n}$$

where

μ_{abs} = average absolute difference between the measurement and model
μ_{rel} = average relative difference between measurement and model
y_i = measurement at depth h_i
x_i = model output at depth h_i

Comparing the absolute and relative differences between the measurements and the model gives a numerical method to estimate the accuracy of the measurement. For the torque comparisons, the model was subtracted from downhole torque measurements. For the drag comparisons, the model was subtracted from the hook load measurements.

From this study, it was determined that a relative difference of 40% is acceptable. Though a relative difference of 40% initially appears to be unacceptably high, given the high amount of uncertainty during drilling operations, a relative difference of 40% is not so unexpected. When relative differences exceed 40%, however, than the outputs are no longer accurately predicting downhole conditions well.

Dataset 1

Dataset 1 is a horizontal well that was drilled in the Gulf of Mexico. It was drilled with an 8 ¾" PDC bit and its BHA contained both a mud motor and an MWD tool. The well's initial trajectory starts as a large vertical section followed by a sudden build-up to

horizontal. A schematic of the wellbore trajectory can be seen in Figure 8 below, while a plot of the plan view can be seen in Figure 9.

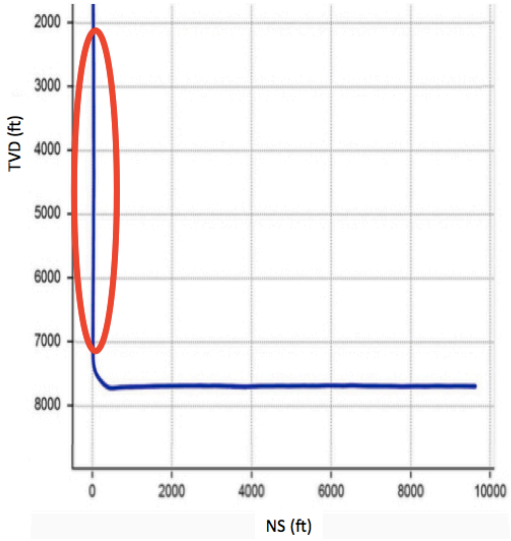

Figure 8: 2-D View of Dataset 1 Wellbore Trajectory. Provided Data Demarcated by Red Ellipse

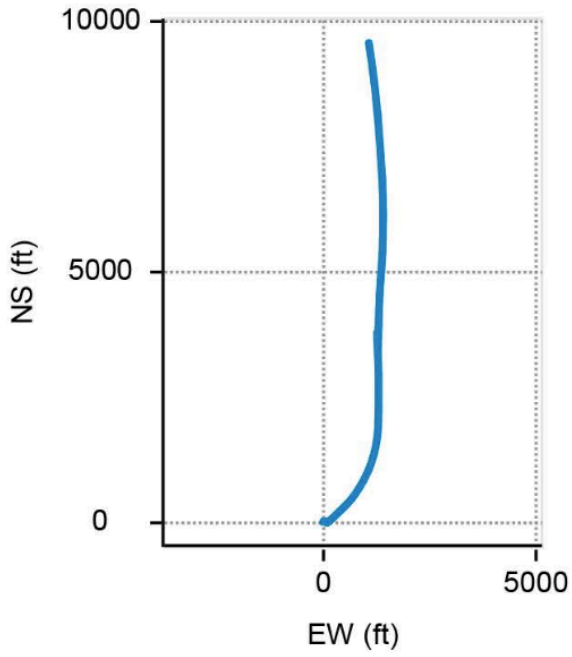

Figure 9: Plan View of Dataset 1

where, in the above figures,

TVD = true vertical depth drilled from surface
NS = distance drilled in North-South direction
EW = distance drilled in East-West direction

The data provided for this project concerns the last half of the vertical section just above the kick-off point, from 2257 to 7129 feet, as noted by the red ellipse in Figure 9 above. This section was drilled with an 8 ¾" PDC bit. The BHA contained a mud motor, MWD tools, and downhole directional tools. The location of the data provided is noted by the red circle on Figure 8 above.

The analyses for Dataset 1 will begin with an examination of the geology that this well was drilled through and then follow with an examination of this well's geometry.

GEOLOGIC ANALYSES FOR DATASET 1

The geology in this dataset consists primarily of sandstones and limestones. A detailed list of the lithologies can be found in Table 1. The lithologies relative to the wellbore trajectory can seen in Figure 10.

Table 1: Dataset 1 Geology		
Lithology	TVD to Top (ft)	TVD to Bottom (ft)
Limestone 1	4257.00	4407.50
Sandstone 1	4407.50	4693.75
Sandstone 2	4693.75	5064.25
Shale 1	5064.25	5404.25
Limestone 2	5404.25	5969.75
Limestone 3	5969.75	6205.50
Sandstone 3	6205.50	6449.75
Sandstone 4	6449.75	6896.75
Sandstone 5	6896.75	7090.50
Sandstone 6	7090.50	7513.75
Limestone 4	7513.75	7549.75
Shale 2	7549.75	7666.75
Sandstone 7	7666.75	7789.75
Limestone 5	7789.75	8005.50
Sandstone 8	8005.50	8073.50
Limestone 6	8073.50	8089.75
Sandstone 9	8089.75	8241.00
Limestone 7	8241.00	8872.75
Limestone 8	8872.75	9129.75

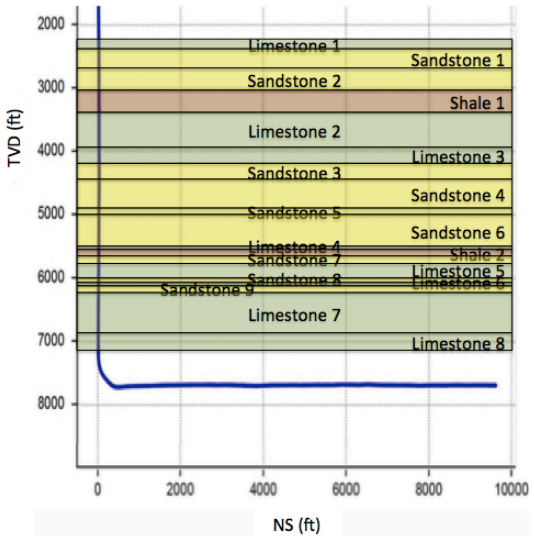

Figure 10: 2-D View of Dataset 1 with Geology

As can be seen from Table 1 and Figure 10, the well was drilled through 19 different formations in the data provided. These formations consist of nine sandstone formations, eight limestone formations, and two shale formations. These formations varied in thickness from 16.25 feet to 631.75 feet. Many of the formations have the same lithology as its neighbor. This allows for interesting analyses, as this allows for comparisons between formations with a similar lithology.

It should be noted that some of the formations with a similar lithology varied by great depths. The bottom of Limestone 3 and the top of Limestone 5 (Limestone 4 is neglected due to its miniscule height) is greater than 1500 feet. Similarly, the distance between the bottom of Sandstone 2 and the top of Sandstone 3 is almost 1150 feet. Thus it should be noted that depth might account for any changes in friction factor.

Unfortunately, Dataset 1 only describes the drilling operations for a vertical section of this well. Because of this, a full analysis on the wellbore trajectory could not be made. A partial analysis was conducted, however, and serves as a baseline comparison for the other analyses.

The first analysis conducted on Dataset 1 is based on the geology of the formation. The results of the drag analysis can be seen in Table 2 and Figure 11 below. The methodology used to construct Figure 11 is discussed in Appendix C.

Table 2: Dataset 1 Drag Friction Analysis by Geology			
Lithology	Optimal Friction Coefficient	Average Absolute Difference (lbs)	Average Relative Difference
Limestone 1	0.31	2779	0.02477
Sandstone 1	0.28	1809	0.01695
Sandstone 2	0.23	1201	0.01064
Shale 1	0.19	1996	0.01667
Limestone 2	0.27	2261	0.01808
Limestone 3	0.26	4493	0.03553
Sandstone 3	0.27	3469	0.02622
Sandstone 4	0.20	5699	0.04114
Sandstone 5	0.18	5405	0.03750
Sandstone 6	0.23	4438	0.03162
Limestone 4	0.31	1629	0.01249
Shale 2	0.26	2149	0.01584
Sandstone 7	0.17	8350	0.05651
Limestone 5	0.25	8119	0.05385
Sandstone 8	0.15	3926	0.02687
Limestone 6	0.27	458	0.00320
Sandstone 9	0.32	7671	0.04713
Limestone 7	0.31	2317	0.01599
Limestone 8	0.30	504	0.00342

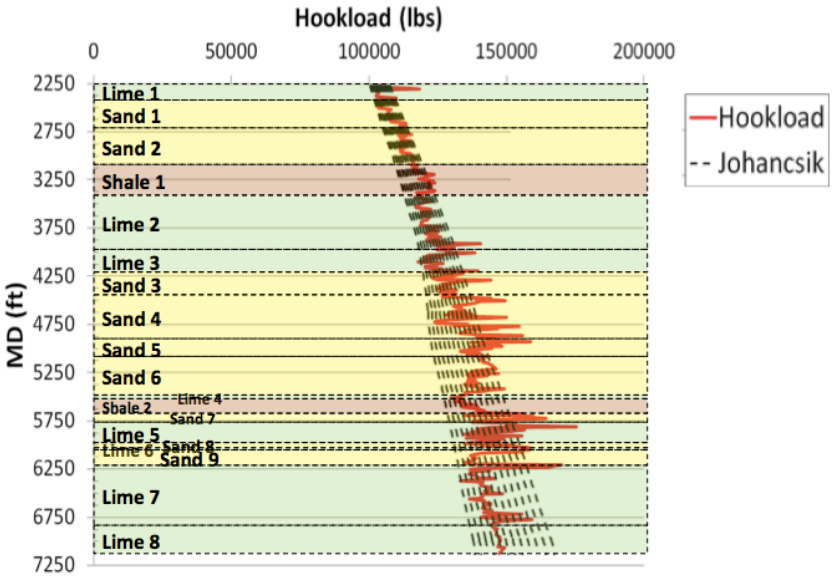

Figure 11: Dataset 1 Hookload Analyses by Geology

where, in the above figures,

MD = total depth drilled from surface

In Figure 11, we have the hookload measurements overlaid by the hookload calculations conducted using Johancsik's model. Johancsik's model was run numerous times with varying friction factors in order to find which factor best describes the drilling data. Each dotted line represents a result from these analyses.

The drag analysis was conducted assuming a traveling block weight of 65000 lbs. When examining the drag data from Dataset 1, it is difficult to draw any conclusions. Overall, the model is capable of accurately predicting the drag losses in order to properly estimate the hookload—the largest relative difference between the model and the measurements for a given formation was in Sandstone 7, which was less than 6%.

The average results of the drag analysis for each lithology can be found in Table 3 below. These results are normalized for height.

Table 3: Summary of Dataset 2 Drag Friction by Lithology

Lithology	Average Friction Factor	Average Absolute Difference (lbs)	Average Relative Difference
Limestone	0.286	2926	0.0216
Shale	0.208	2035	0.0165
Sandstone	0.231	4220	0.0304

From Table 3, we see that limestone tended to have the highest drag friction factor, followed by sandstones and then shale. Sandstones, however, tended to have the largest differences between the model calculations and downhole measurements. Limestone had the second largest difference and shales tended to be most accurately predicted by Johancsik's model.

The results of the torque analyses conducted on Dataset 1 are found in Figure 12 and Table 4 below.

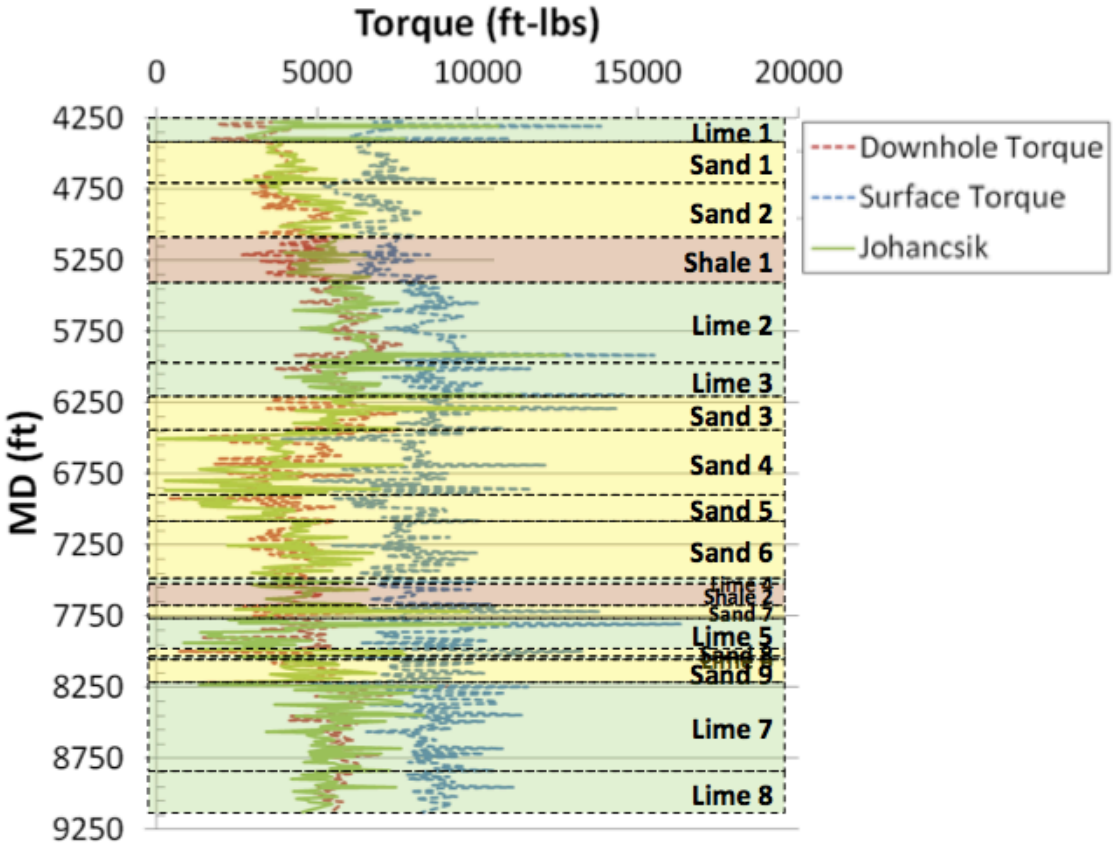

Figure 12: Dataset 1 Torque Analyses by Geology

Table 4: Dataset 1 Torque Friction by Geology			
Lithology	Optimal Friction Coefficient	Average Absolute Difference (lbs)	Average Relative Difference
Limestone 1	0.42	1632	0.725
Sandstone 1	0.34	362	0.097
Sandstone 2	0.24	441	0.116
Shale 1	0.24	584	0.156
Limestone 2	0.20	808	0.149
Limestone 3	0.20	1057	0.207
Sandstone 3	0.18	1344	0.302
Sandstone 4	0.22	1470	0.424
Sandstone 5	0.21	1333	0.363
Sandstone 6	0.13	701	0.182
Limestone 4	0.14	592	0.125
Shale 2	0.11	234	0.048
Sandstone 7	0.15	1631	0.428
Limestone 5	0.20	2447	1.016
Sandstone 8	0.11	1351	0.296
Limestone 6	0.23	116	0.032
Sandstone 9	0.10	951	0.234
Limestone 7	0.08	800	0.139
Limestone 8	0.09	512	0.096

From Figure 12, it can be seen that the relative difference between the model's outputs and the downhole measurements are less than 40%. Thus, as stated above, the model predicts the downhole torque measurements within the acceptable accuracy. The model followed the trend of the downhole torque measurements. A few formations were less accurate than other formations, but overall, the model was able to capture the overarching trends in the downhole torque measurements.

A summary of Table 4 can be found in Table 5, which averages the friction factor and the absolute and relative differences for each lithology and normalizes by formation height.

Table 5: Summary of Dataset 1 Torque Friction by Lithology			
Lithology	Average Friction Factor	Average Absolute Difference (ft-lbs)	Average Relative Difference
Limestone	0.165	1015	0.275
Shale	0.207	495	0.129
Sandstone	0.202	972	0.255

From Table 5, it can be seen that all the formations had about the same torque friction factor, with limestone having a slightly smaller torque friction factor than sandstone and shale. Limestone and sandstone tended to be predicted by Johancsik's model with equal accuracy, while shale being predicted with slightly higher accuracy.

GEOMETRIC ANALYSES FOR DATASET 1

As stated above, this dataset describes only the vertical portion of this wellbore. As such, extensive geometric analyses could not be conducted on this dataset. Nevertheless, an analysis could be run on the overall dataset and compared to similar geometries in the other datasets. The dataset's geometry is described in Table 6 and Figure 13 below.

Table 6: Dataset 1 Wellbore Trajectory		
Geometry	MD to Top (ft)	MD to Bottom (ft)
Vertical	2257	7130

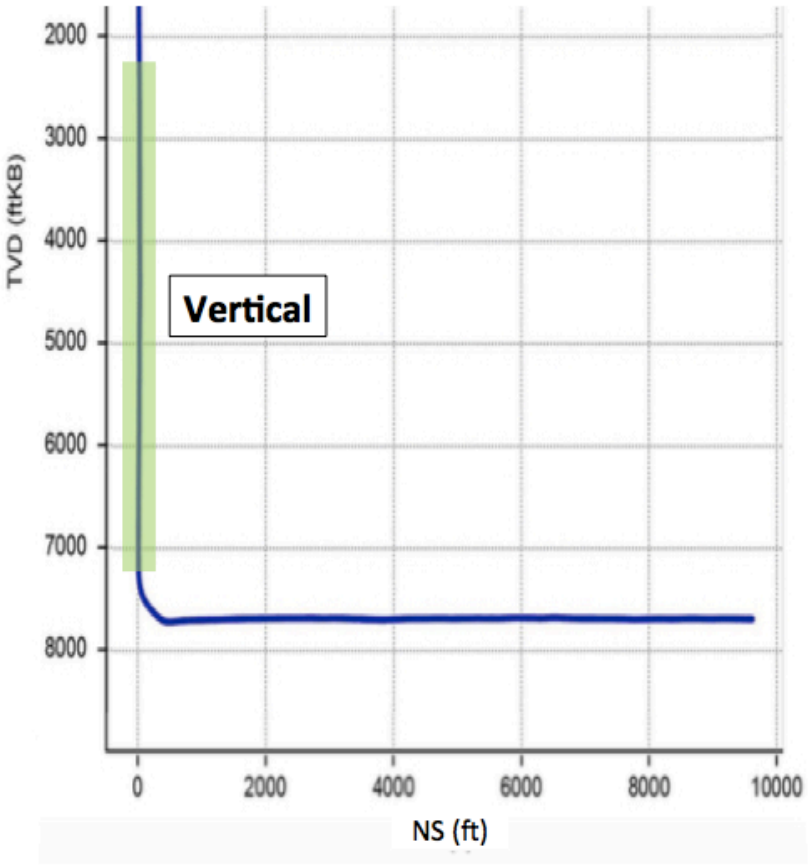

Figure 13: Dataset 2 Wellbore Trajectory with Marked Geometry

For this dataset, a drag analysis will be conducted followed by a torque analysis. The results of the drag analysis are found in Table 7and Figure 14 below.

Table 7: Dataset 1 Drag Friction Analysis by Geometry			
Geometry	Optimal Friction Coefficient	Average Absolute Difference (lbs)	Average Relative Difference
Vertical	0.27	4959	0.0358

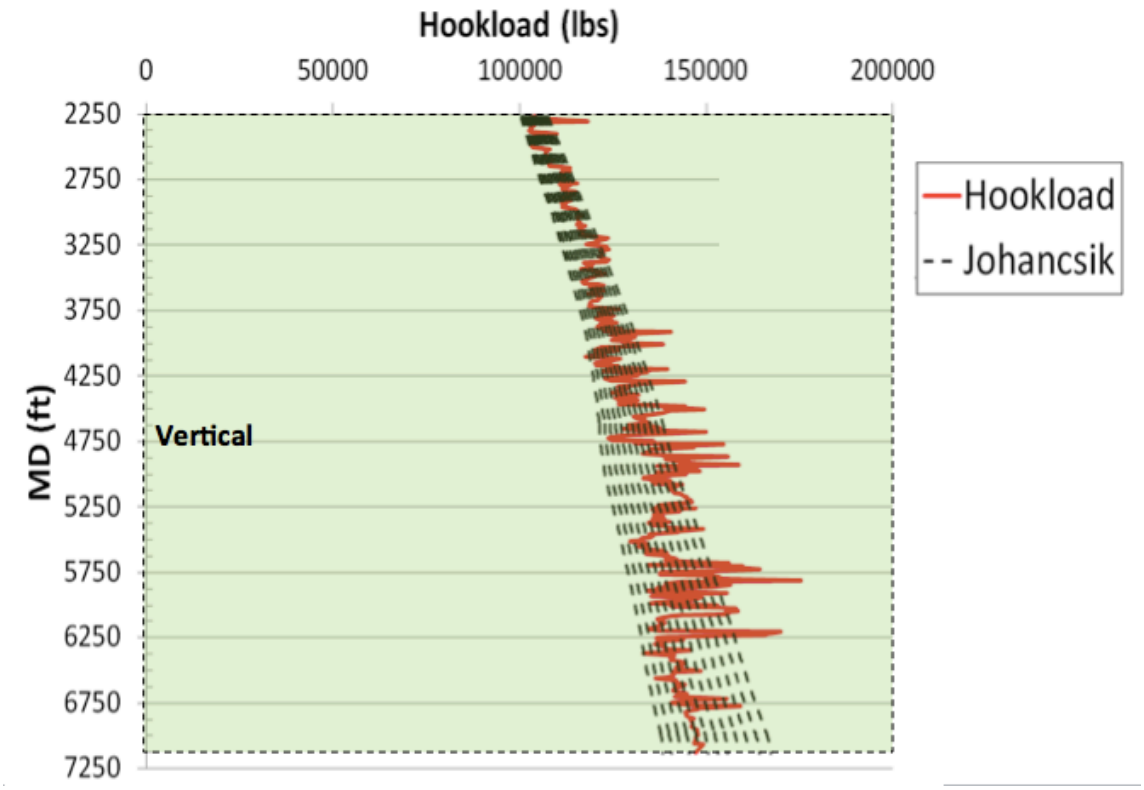

Figure 14: Dataset 1 Drag Friction Analyses by Geometry

From Table 7 and Figure 14, it can be seen that this well has a fairly typical drag friction coefficient. Because this dataset contains only the vertical section, it can only be compared to the datasets. Nevertheless, Johancsik's model was able to predict the drag friction factor of Dataset 1 accurately, with an average relative difference between the model and the measurements of less than 4%.

The results of the torque friction analysis on this section can be found in Table 8 and Figure 15 below.

Table 8: Dataset 2 Torque Friction Analysis by Geometry			
Geometry	Optimal Friction Coefficient	Average Absolute Difference (ft-lbs)	Average Relative Difference
Vertical	0.15	1430	0.3775

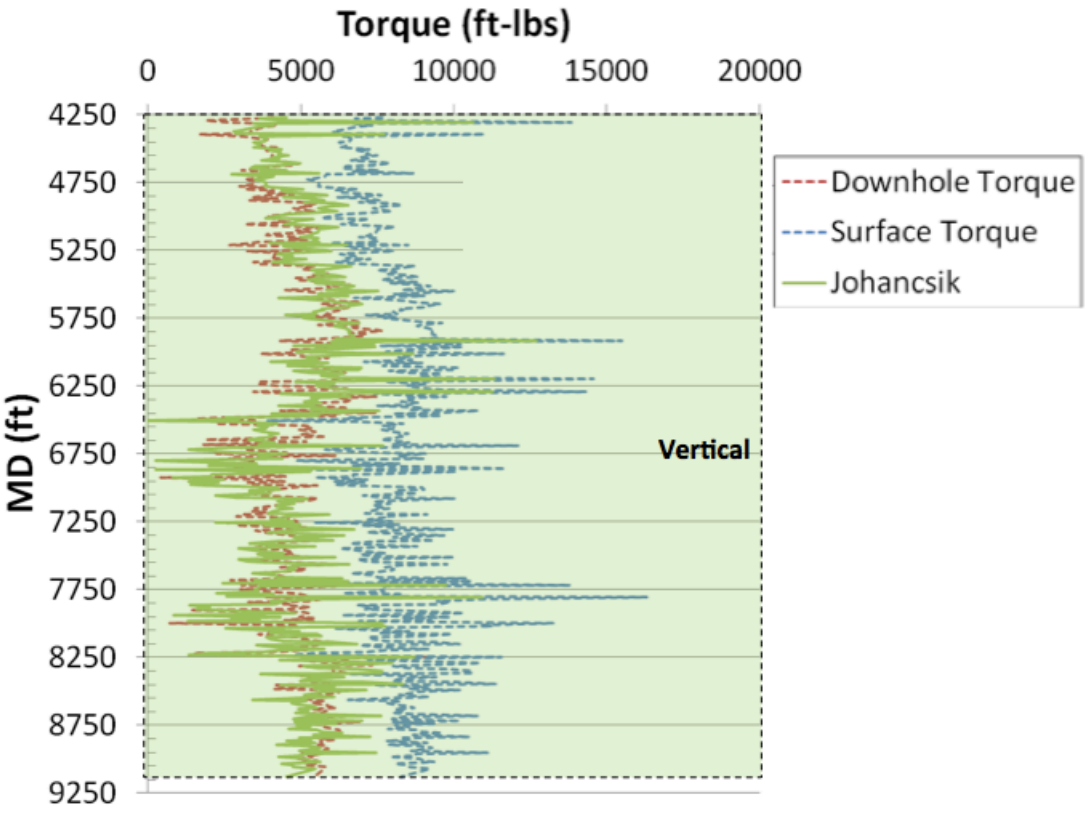

Figure 15: Dataset 2 Torque Friction Analyses by Geometry

Again, because this dataset only contains one wellbore geometry and thus this analysis cannot be compared to other geometries without comparing to another dataset. But nevertheless, the torque friction coefficient is a fairly typical value. The model was able to predict torque friction factor with accuracy, capturing the general trends of the downhole measurements. It should be noted that the average relative difference in the torque analysis is much higher than the average relative difference in the drag analysis.

This is because Johancsik's model depends on the surface torque measurements in order to conduct an analysis. For a drag analysis, the model calculates the hookload directly and does not require any surface measurements.

Dataset 2

The second dataset provided by our sponsors is of a south Texas well. This well was drilled using four different drill bits and BHA configurations. The first drill bit was a 12 ¼" PDC bit. The first BHA contained a downhole motor, a stabilizer, and MWD tools. The second BHA contained an 8 ¾" PDC bit, downhole motor, and a MWD tool. The third BHA used an 8 ½" PDC bit, had a stabilizer, a rotary steerable system, and a MWD tool. The fourth and final BHA used an 8.5" PDC bit, a rotary steerable system, and a MWD tool.

A schematic of the well geometry can be seen in Figure 16 below.

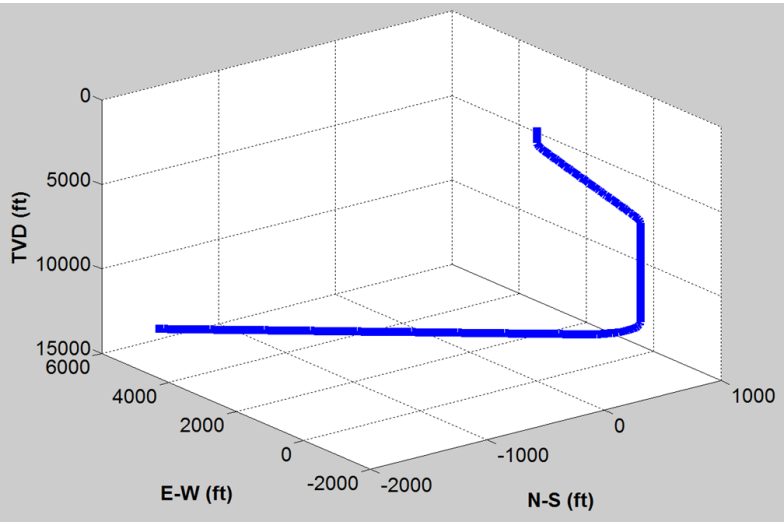

Figure 16: 3-D View of Dataset 2

From Figure 16, we see that the well starts with an initial 10° slant that lasts for about the first 7000 feet drilled. After this slant, there is a vertical section, followed by a buildup into a long horizontal section. A 2-D view of the trajectory as well as the corresponding geology can be seen in Figure 17.

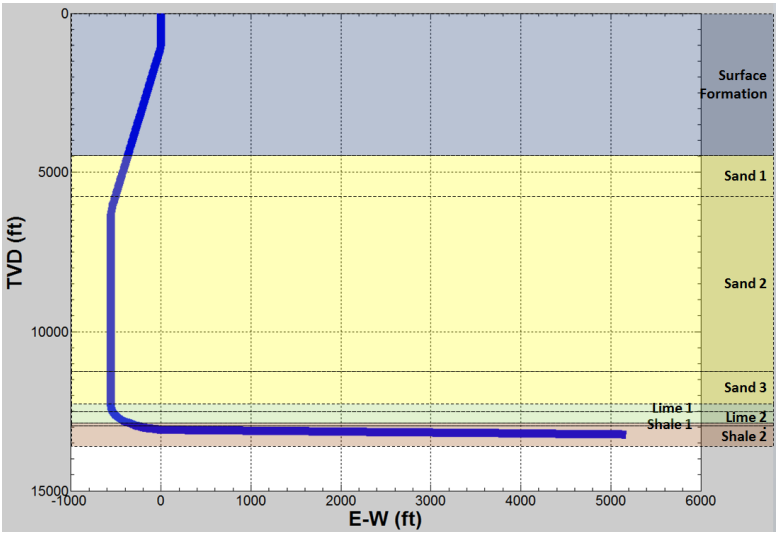

Figure 17: 2-D View of Dataset 2 with Geology

From Figure 17, we see that the well was drill through three large sandstones followed by two smaller limestones and two shales. The geology is described in Table 9 below.

Table 9: Dataset 2 Geology

Formation	TVD to Top (ft)	TVD to Bottom (ft)
Surface Formation	0	4492
Sandstone 1	4492	5707
Sandstone 2	5707	11287
Sandstone 3	11287	12304
Limestone 1	12304	12526
Limestone 2	12526	12924
Shale 1	12924	12982
Shale 2	12982	13165

From Table 9, we see that this well was drilled through a fairly constant geology, with the largest formation being more than 5000 feet thick. The smallest formation, however, is only 58 feet thick.

The wellbore geometry coincided with the geology. As can be viewed in Figure 17, the initial downward slant was drilled in through the surface formation and Sand 1. Afterwards, the trajectory built-up into a vertical section in Sand 2 and Sand 3, and then started building up again in Limestone 1 and Limestone 2. This culminated into a long horizontal section in Shale 2.

Dataset 2 will first be analyzed by geology and then by wellbore trajectory.

GEOLOGIC ANALYSES FOR DATASET 2

The results of the drag analysis by geology are given in Table 10 and Figure 18 below.

Table 10: Dataset 2 Drag Friction Analysis by Geology

Lithology	Optimal Friction Coefficient	Average Absolute Difference (lbs)	Average Relative Difference
Surface	0.45	3364	0.0588
Sandstone 1	0.38	4576	0.0423
Sandstone 2	0.18	6439	0.0405
Sandstone 3	0.14	2370	0.0110
Limestone 1	0.19	4008	0.0191
Limestone 2	0.15	1559	0.0069
Shale 1	0.22	34	0.0002
Shale 2	0.18	7563	0.0353

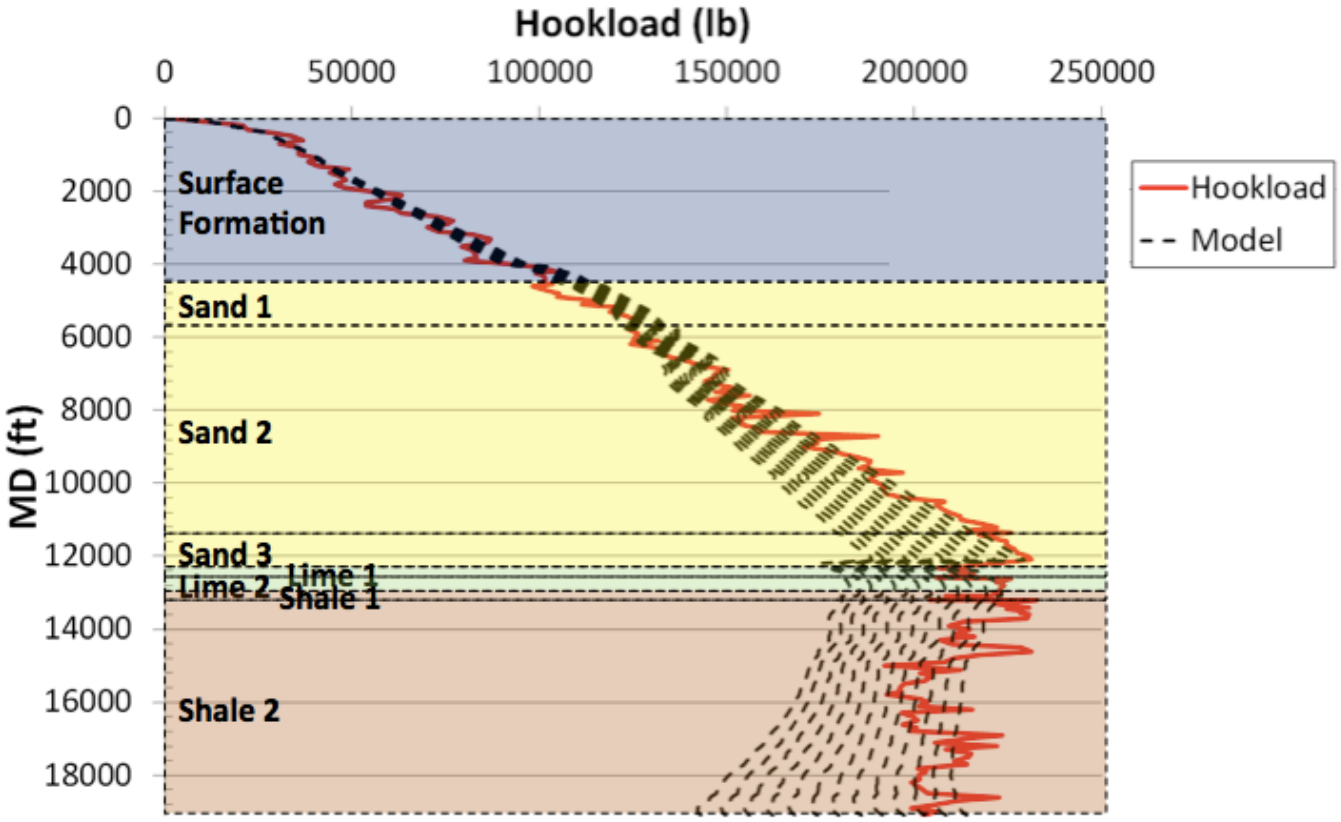

Figure 18: Dataset 2 Hookload Analyses by Geology

Like Dataset 1, this drag analysis was conducted assuming a traveling block weight of 65000 lbs. From the above analyses, we see that the friction factors overall did not vary significantly from one another, except for Sandstone 1. Sandstone 1had a significantly higher friction factor than all the other formations other than the surface formation.

Johancsik's model was able to accurately predict the drag friction losses experienced during the drilling process for this dataset. The model was able to accurately predict the friction losses to within 6% of the downhole measurement for all formations.

The error was within about 4% for sandstones, 3.5% for shales, and 2% for limestones. The 6% relative difference was in the surface formation.

A summary normalized by formation height of Table 10 and Figure 18 is given in Table 11 below.

Table 11: Summary of Dataset 2 Drag Friction by Lithology			
Lithology	Average Friction Factor	Average Absolute Difference (lbs)	Average Relative Difference
Surface Formation	0.450	3364	0.0588
Sandstone	0.206	5615	0.0369
Limestone	0.163	2339	0.0108
Shale	0.181	7435	0.0347

From Table 11, we see that sandstones, excluding the initial surface formation, had the highest friction factor, but only by a small margin. Limestone has the next smallest friction factor and shale was in between the two. Confirming what was seen in Table 7, it can be seen that Johancsik's model as able to accurately estimate the friction losses on the drill string, with relative differences of less than 4% for shales and sandstones and at about 1% for limestones. It is interesting to note that the relative difference for limestones is about a third of the relative difference of sandstones and shales. This may be due to reasonable variance, however, as the relative differences for all lithologies were small.

The results of the torque analysis, by geology, are given in Table 12 and Figure19 below.

Table 12: Dataset 2 Torque Friction Analyses by Geology			
Lithology	Optimal Friction Coefficient	Average Absolute Difference (ft-lbs)	Average Relative Difference
Surface Formation	0.35	965	0.4239
Sandstone 1	0.54	519	0.4406
Sandstone 2	0.48	1495	0.7135
Shale 2	0.18	972	0.3835

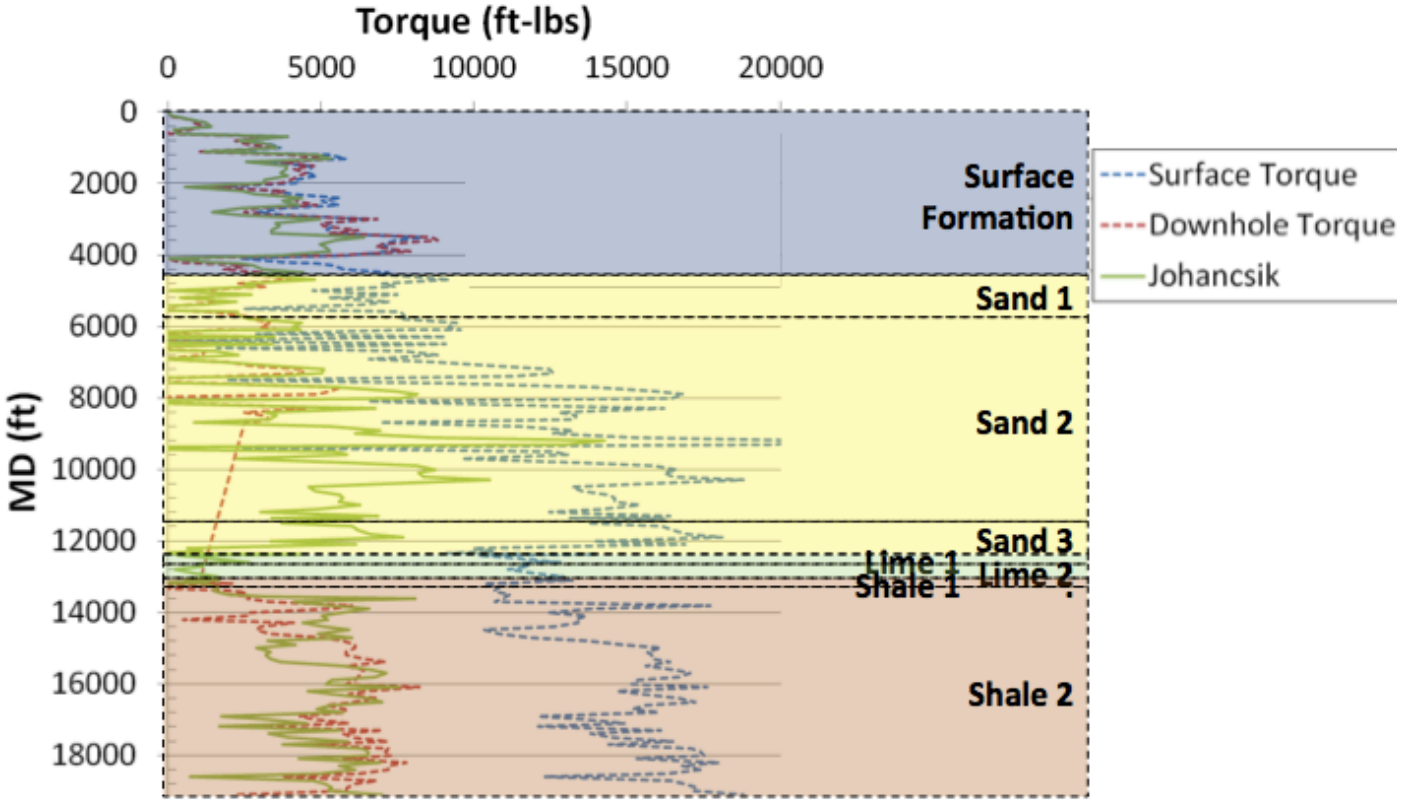

Figure 19: Dataset 2 Torque Analyses by Geology

From Figure 19, it can be seen that there were issues with the downhole measurement tool between 8635 and 13197 feet. Because of this, torque analyses could not be conducted in this interval. The formations in this interval are part of Sandstone 2,

Sandestone 3, Limestone 1, Limestone 2, and Shale 1. The results of the analyses that could be conducted are shown in Table 12 above.

From the analyses that were able to be conducted, it can be seen that the initial two sandstones had a significantly higher torque friction factor than did Shale 2. Along similar lines, the sandstones also had a much larger relative difference between the model's output and the downhole measurements. If the analyzed lithologies are normalized by formation height, we see that this is the case. This summary of the torque analyses for Dataset 2 can be found in Table 13 below.

Table 13: Summary of Dataset 2 Torque Friction by Lithology

Lithology	Average Friction Factor	Average Absolute Difference (ft-lbs)	Average Relative Difference
Surface Formation	0.350	965	0.4239
Sandstone	0.498	1200	0.6310
Shale	0.180	972	0.3835

From Table 13, we see that the sandstones on average have a significantly higher friction factor than Shale 2 or Surface Formation. It also tended to be less accurately predicted by Johancsik's model. Some of the error may be attributed to the downhole tool malfunctioning before it went offline.

GEOMETRIC ANALYSES FOR DATASET 2

From Figure 17, it can be seen that the wellbore trajectory from Dataset 2 can be divided into seven distinct sections. It starts with a short vertical section for 200 feet, followed by a build-up into a downward slant for 5900 feet. It then draws-down into a

5300-foot vertical section. Finally, the well builds into a 5500-foot horizontal section. These sections are described in Table 14 and marked in Figure 20 below.

Table 14: Dataset 2 Wellbore Trajectory		
Geometry	MD to Top (ft)	MD to Bottom (ft)
Vertical 1	0	200
Build-up 1	200	1300
Downward Slant	1300	6100
Draw-down	6100	7000
Vertical 2	7000	12300
Build-up 2	12300	13500
Horizontal	13500	19100

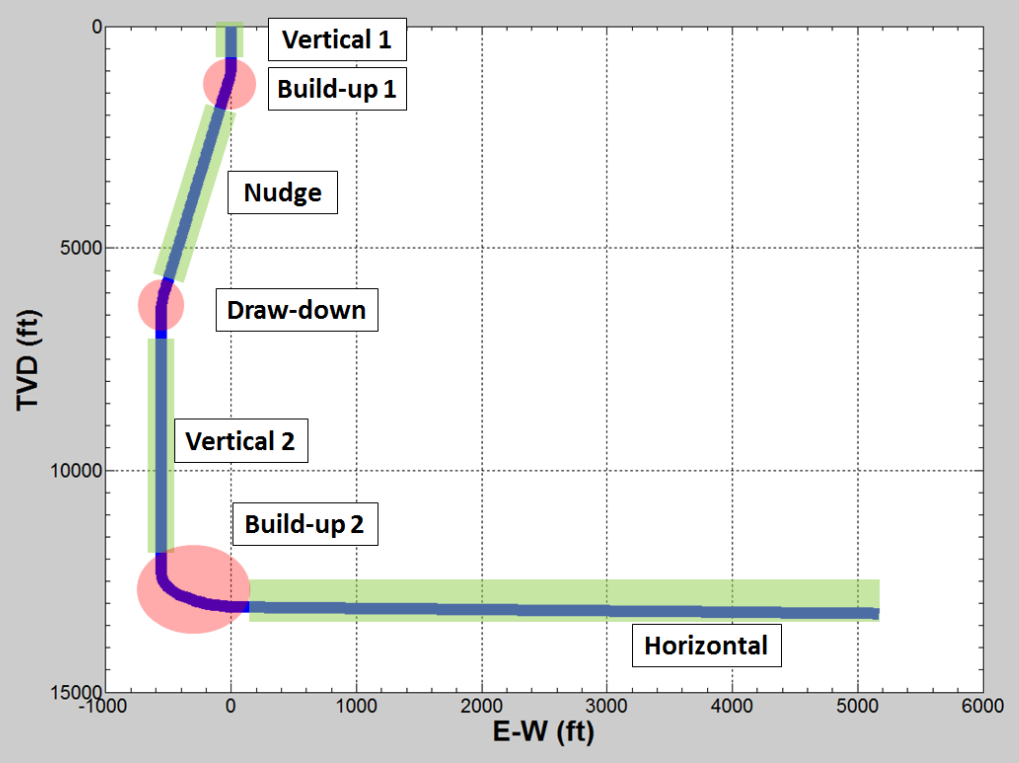

Figure 20: 2-D View of Dataset 2 Wellbore Trajectory with Marked Geometry

A drag analysis was conducted on each wellbore section and is given in Table 15 and Figure 21 below.

Table 15: Dataset 2 Drag Friction Analysis by Geometry			
Geometry	Optimal Friction Coefficient	Average Absolute Difference (lbs)	Average Relative Difference
Vertical 1*	*	1710	0.0858
Build-up 1	0.84	2242	0.0643
Downward Slant	0.42	3907	0.0480
Draw-down	0.31	4334	0.0309
Vertical 2	0.15	5416	0.0313
Build-up 2	0.15	5991	0.0278
Horizontal	0.18	7016	0.0330

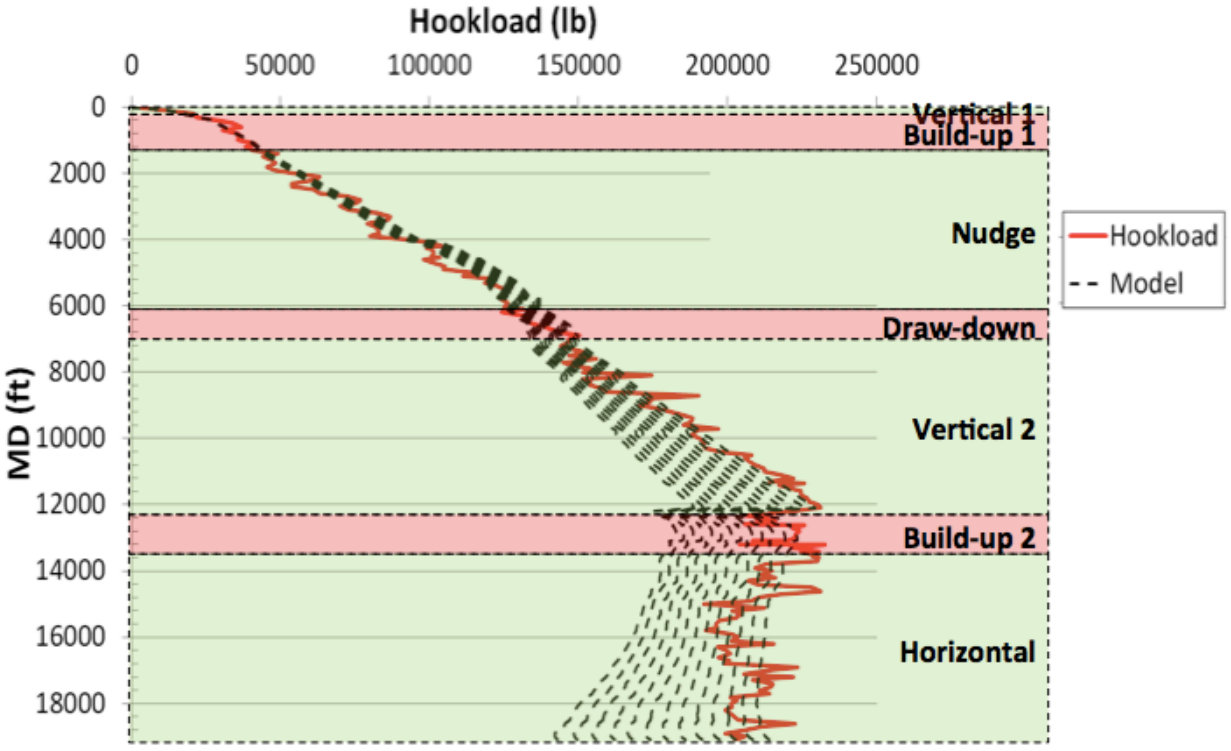

Figure 21: Dataset 2 Hookload Analyses by Geometry

It is important to note that Vertical 1, due to its containing only 2 data points, could not be properly analyzed.

But disregarding Vertical 1, it can be seen that, curiously, the drilling operation initially had a very high drag friction coefficient that slowly that gradually decreased as

the drilling operation continued. After recording a coefficient of 0.84, the model eventually stabilized at a much more typical coefficient of about 0.18. It is interesting to note that the higher friction cofficients coincided with going into and eventually drilling out of the initial downward slant, while the lower coefficients coincided with the horizontal section.

Overall, Johancsik's model was able to accurately estimate the drag friction losses for this well. The model maintained within 9% of the downhole measurements for every section and within 6.5% if Vertical 1 is ignored due to its having too few data points.

The torque results are given in Table 16 and Figure 22 below.

Table 16: Dataset 2 Torque Friction Analysis by Geometry

Geometry	Optimal Friction Coefficient	Average Absolute Difference (ft-lbs)	Average Relative Difference
Vertical 1*	*	114	1.0204
Build-up 1	0.65	376	0.4120
Downward Slant	0.36	1357	0.6274
Draw-down	0.48	1433	1.0950
Vertical 2**	0.51	1655	0.5944
Build-up 2**	0.18	1022	0.8767
Horizontal	0.18	900	0.3149

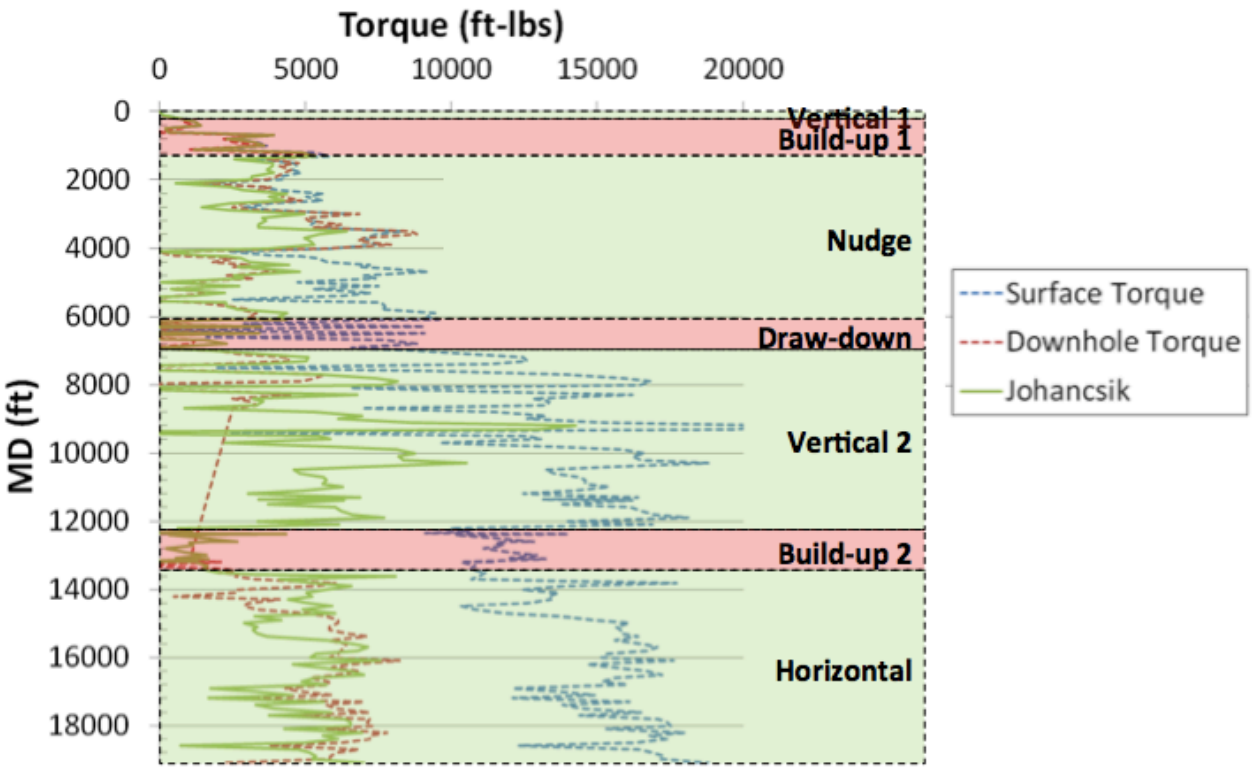

Figure 22: Dataset 2 Torque Friction Analyses by Geometry

Again, Vertical 1 could not be properly analyzed due to the small sample size of its dataset. Also, as with the previous geologic analyses, some of the torque analyses for Dataset 2 could not be conducted due to a failure in the downhole MWD tool between 8635 and 13197 feet md. This failure prevented the MWD from recording any measurements during this interval. This interval coincides with the majority of Vertical 2 and Build-up 2. Partial analyses were conducted on these two sections while full analyses were conducted on the rest of the wellbore other than Vertical 1. Furthermore, the downhole measurements for Draw-down gave several zero and negative measurements. This suggests either that the either the downhole MWD tool was beginning to fail before

it stopped recording measurements or that the operator was experiencing difficulties during their drilling operation and explains the large relative and absolute differences between the model and the measurements in this section. That the MWD tool began to malfunction in Draw-down is corroborated by Table 13, as Draw-down has a large average relative difference between the measurement and model output.

From Table 16, it can be seen that the well has a large drag friction coefficient for all of the initial sections that were analyzed. Up to Vertical 2, the smallest friction coefficient belonged to Downward Slant and was still significantly higher than was estimated in the previous analyses. After the malfunctioning MWD was repaired, the friction coefficients decreased significantly. The friction coefficient in both Build-up 2 and Horizontal were estimated to be 0.18, which is half of the smallest torque friction coefficient that was previously recorded for this well. One explanation of this is that the malfunctioning MWD tool led to incorrect downhole torque measurements and that this was corrected after the MWD tool was fixed. This suggestion is corroborated with the fact that average relative difference between the model and the downhole measurement decreased significantly in the horizontal section.

It can be seen from Figure 22 that Johancsik's model correctly follows the trend of the downhole torque measurements. The largest deviations from the model outputs and downhole measurements appear to be caused by outliers in the surface measurements. Otherwise it appears that the model is able to follow the trends of the actual downhole

measurements. The large average relative difference between the downhole measurements and model can largely be explained by the malfunctioning downhole tool.

Dataset 3

Like Dataset 2, the third dataset provided by our sponsors describes a south Texas well. It was drilled using three different BHA's. The first BHA contained a 12 ¼" PDC drill bit, a downhole motor, a stabilizer, and a MWD tool. The second BHA contained an 8 ¾" PDC bit, a dowhole motor, a stabilizer, and a MWD tool. Finally, the third downhole BHA contained an 8 1/2" PDC drill bit, a rotary steerable system, a HEL tool, and a MWD tool.

A 3-D schematic of the wellbore trajectory is given in Figure 23 below.

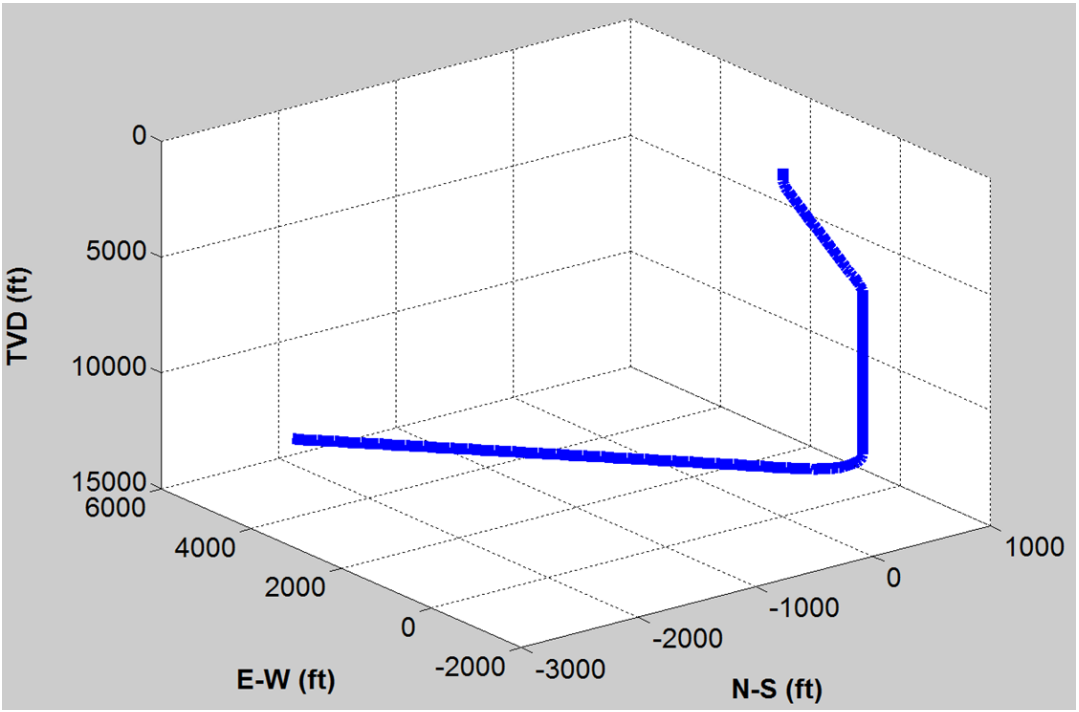

Figure 23: 3-D View of Dataset 3

As can be seen from Figure 13, this well has a similar trajectory as Dataset 2. This well also starts with an initial 10° downward slant into a vertical section into a long horizontal section. A 2-D trajectory, along with the geology of formations that were drilled, is shown in Figure 24 below.

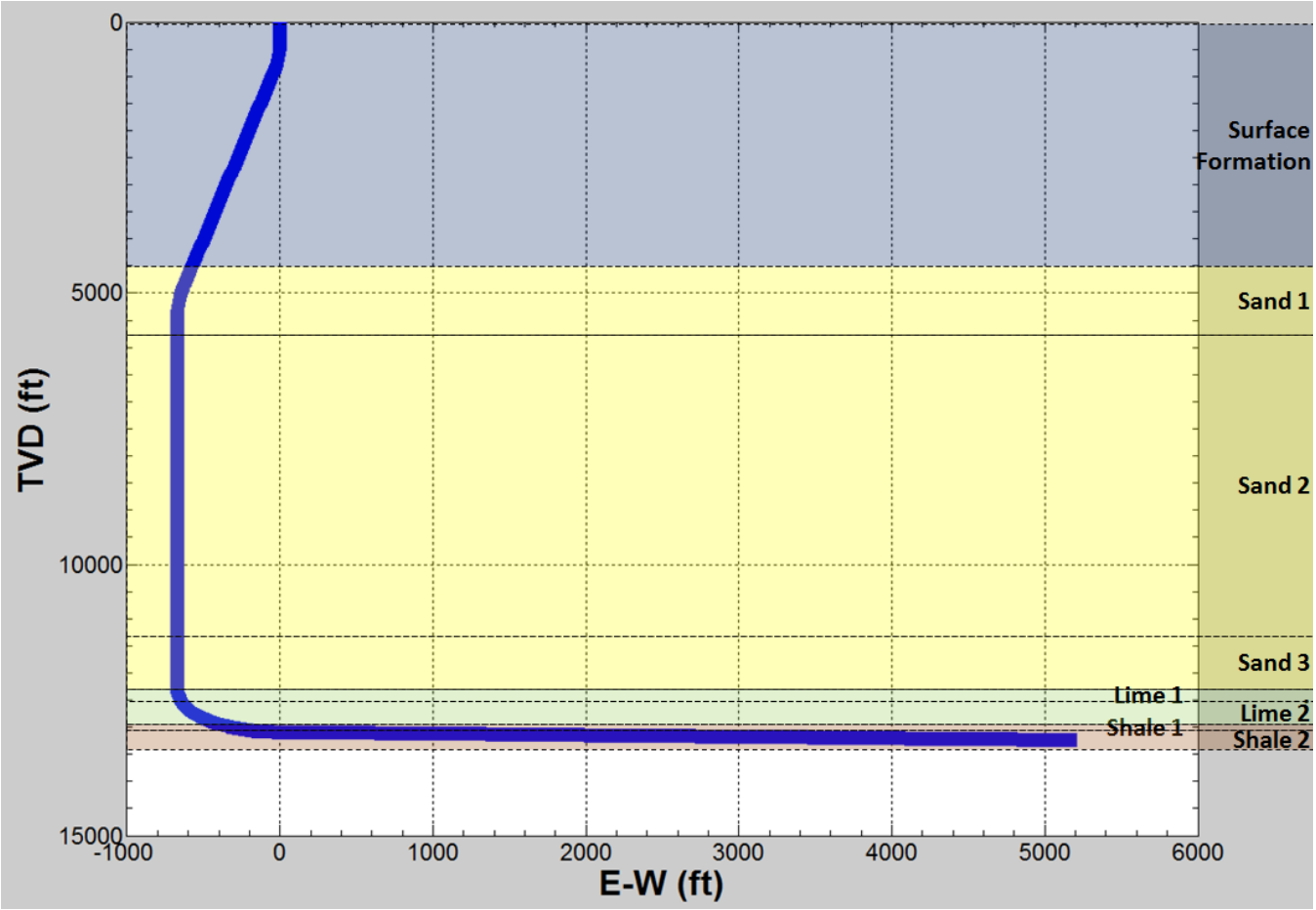

Figure 24: 2-D View of Dataset 3 with Geology

As shown in Figure 24, this well was drilled through geology similar to Dataset 2's geology. Like Dataset 2, this geology also consists of three sandstones, two limestones, and two shales. The geology is given in Table 17 below.

Table 17: Dataset 3 Geology		
Formation	TVD to Top (ft)	TVD to Bottom (ft)
Surface Formation	0	4493
Sandstone 1	4494	5706
Sandstone 2	5707	11321
Sandstone 3	11322	12308
Limestone 1	12309	12531
Limestone 2	12532	12930
Shale 1	12931	12987
Shale 2	12988	13168

Again, this well was drilled with a fairly consistent geology. It was drilled through three consecutive sandstones, followed by two consecutive limestones and then consecutive shales. And again, this well's geometry coincides with the geology. As can be seen from Figure 24, the downward slant draws down to a vertical section in Sandstone 1, and then in Limestone 1 the vertical section builds up until the horizontal section in Shale 2.

Dataset 3 will be analyzed first by geology and then by geometry.

GEOLOGIC ANALYSES FOR DATASET 3

The first geology analysis for Dataset 3 is a drag friction analysis conducted on this wellbore. These analyses were conducted assuming a traveling block weight of 60,000 lbs. The results of this analysis for Dataset 3 by geology are given in Table 18 and Figure 25 below.

Table 18: Dataset 3 Drag Friction Analysis by Geology			
Lithology	Optimal Friction Coefficient	Average Absolute Difference (lbs)	Average Relative Difference
Surface Formation	0.00	7619	0.1274
Sandstone 1	0.38	4636	0.0389
Sandstone 2	0.18	7041	0.0428
Sandstone 3	0.15	4248	0.0196
Limestone 1	0.19	6007	0.0260
Limestone 2	0.17	3651	0.0159
Shale 1	0.16	341	0.0015
Shale 2	0.23	9543	0.0461

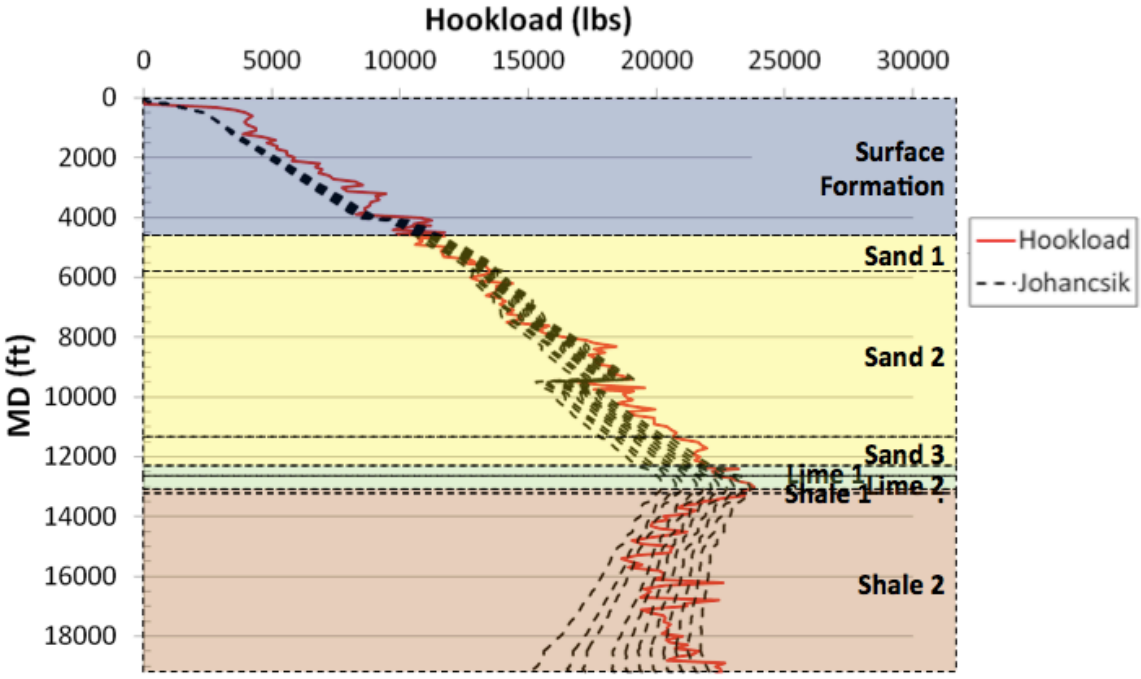

Figure 25: Dataset 3 Drag Analyses by Geology

Note that the jump in the model's hookload from 4069 to 9423 feet md is due to a change in BHA. The second BHA used significantly more heavy-weight drill pipe, leading to a much heavier predicted hookload.

From Table 18 and Figure 25, it can be seen that this dataset has a very low drag friction coefficient in all formations except for Sandstone 1. Other than Sandstone 1, the friction coefficients for all formations were smaller than 0.24. In fact, other than Sandstone 1 and Shale 2 (through which the entire horizontal section is drilled), no formation had a friction coefficient larger than 0.19.

Overall, it appears that Johancsik's model was able to accurately predict the friction losses in all formations, with small relative differences between the model output and the hookload measurements for all formations. The model was least able to predict the drag friction losses in Surface Formation but was still able to be within 13% of the measurements for that formation. For every other formation, the model was able to predict the hookload to within 5%.

A summary of the above analyses, after normalizing by height, can be found in Table 19 below.

Table 19: Summary of Dataset 3 Drag Friction by Lithology

Lithology	Average Friction Factor	Average Absolute Difference (lbs)	Average Relative Difference
Surface Formation	0.000	7619	0.1274
Sandstone	0.207	6311	0.0393
Limestone	0.176	4398	0.0191
Shale	0.229	9387	0.0454

From Table 19, it can be seen that the average friction factor for all lithologies are about the same. Unlike in Dataset 2, where sandstone had the highest friction coefficients, it is shale that has a slightly friction coefficient in Dataset 3. Sandstone has the second largest friction coefficient and limestone has the smallest. And confirming

what was stated above, from Table 19, it can be shown that Johancsik's model was able to accurately predict the hookload to within 5% for all formations. It is interesting to note that, like in Dataset 2, the relative difference of limestone is smaller than the relative difference of sandstone and shale. Johancsik's model predicts the drag friction factor for sandstone and shale with about the same accuracy, but is slightly more accurate at predicting limestone.

The results of the Dataset 3 torque analyses by geology are shown in Table 20 and Figure 26 below.

Table 20: Dataset 3 Torque Friction Analyses by Geology

Formation	Optimal Friction Coefficient	Average Absolute Difference (ft-lbs)	Average Relative Difference
Surface Formation**	0.23	475	0.2725
Sandstone 2**	0.29	1749	0.7356
Sandstone 3	0.30	572	0.3432
Limestone 1	0.38	2206	1.3821
Limestone 2	0.17	703	0.3121
Shale 1	0.20	39	0.0149
Shale 2	0.24	1773	0.9813

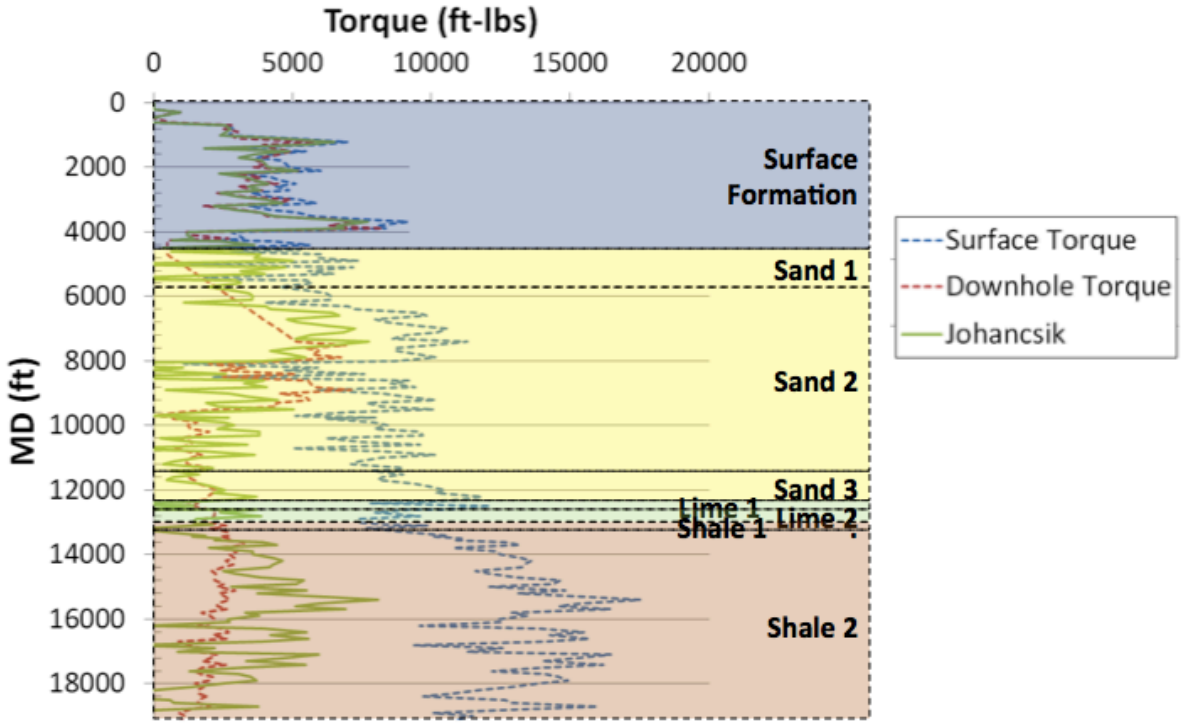

Figure 26: Dataset 3 Torque Analyses by Geology

It should be noted that, as in Dataset 2, this well also had issues with its downhole MWD tool. This time, the malfunction occurred between 4136 and 7631 ft md. This coincides with the end of Surface Formation, through the entirety of Sandstone 1, and about a third of Sandstone 2. Due to this malfunction, torque analyses could not be conducted in this interval.

From Table 20 and Figure 26, it can be seen that sandstone has a relatively high torque friction factor while shale has a relatively low torque friction factor. Interestingly, there is a large disparity between the friction coefficients of Limestone 1 and Limestone 2. This may be explained by the surface torque measurements being erratic in Limestone 1. The high average relative difference and average absolute difference between the

downhole measurements and model output in Limestone 1 corroborate that something unexpected was occurring in this formation. Other than Limestone 1 and Shale 2, the Johancsik's model is able to predict the downhole torque measurements. The model was certainly able to identify the general trends of the downhole measurements.

A summary of the Dataset 3 torque analyses by geology can be found in Table 21 below. This summary has been normalized for the height of each formation.

Table 21: Summary of Dataset 3 Torque Friction by Lithology

Lithology	Average Friction Factor	Average Absolute Difference (ft-lbs)	Average Relative Difference
Surface Formation	0.230	475	0.2725
Sandstone	0.292	1504	0.6538
Limestone	0.237	1181	0.6531
Shale	0.239	1743	0.9650

From Table 21, it can be seen that the lithologies have similar torque friction factors. The shale and limestone torque friction factors are almost identical, and the sandstone friction factor is only about 20% larger than these. Johancsik's model estimated sandstone and limestone friction factors with almost equal accuracy, but was slightly less accurate at predicting shale friction factors. Overall, however, there does not appear to be a large difference between the drag friction factors of each lithology.

GEOMETRIC ANALYSES FOR DATASET 3

From Figure 24, it can be seen that well described in Dataset 3 has a very similar geometry to the well described in Dataset 2. Like Dataset 2, this well starts with a very short vertical section that builds into a downward slant that draws down into a vertical

section that builds into a long horizontal section. The complete geometry is described in Table 22 and Figure 27 below.

Table 22: Dataset 2 Wellbore Trajectory		
Geometry	MD to Top (ft)	MD to Bottom (ft)
Vertical 1	0	200
Build-up 1	200	900
Downward Slant	900	4700
Draw-down	4700	5700
Vertical 2	5700	12100
Build-up 2	12100	13500
Horizontal	13500	19124

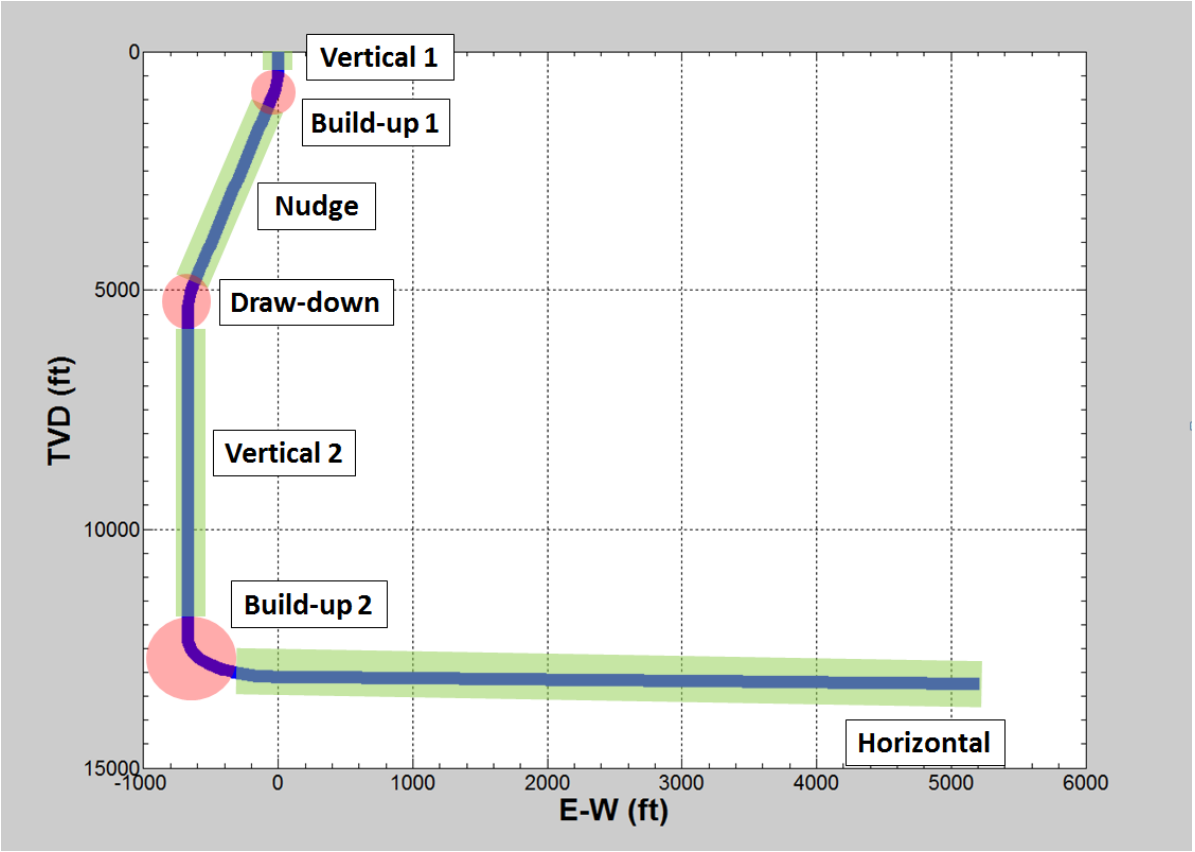

Figure 27: 2-D View of Dataset 2 Wellbore Trajectory with Marked Geometry

A drag analysis was conducted on each of the above wellbore sections. The results of these analyses are shown in Table 23 and Figure 28 below.

Table 23: Dataset 3 Drag Friction Analysis by Geometry			
Geometry	Optimal Friction Coefficient	Average Absolute Difference (lbs)	Average Relative Difference
Vertical 1*	*	0	0.0000
Build-up 1	0	14334	0.3870
Slant	0	7316	0.0966
Draw-down	0.38	3818	0.0315
Vertical 2	0.15	6599	0.0408
Build-up 2	0.17	3309	0.0145
Horizontal	0.24	9803	0.0475

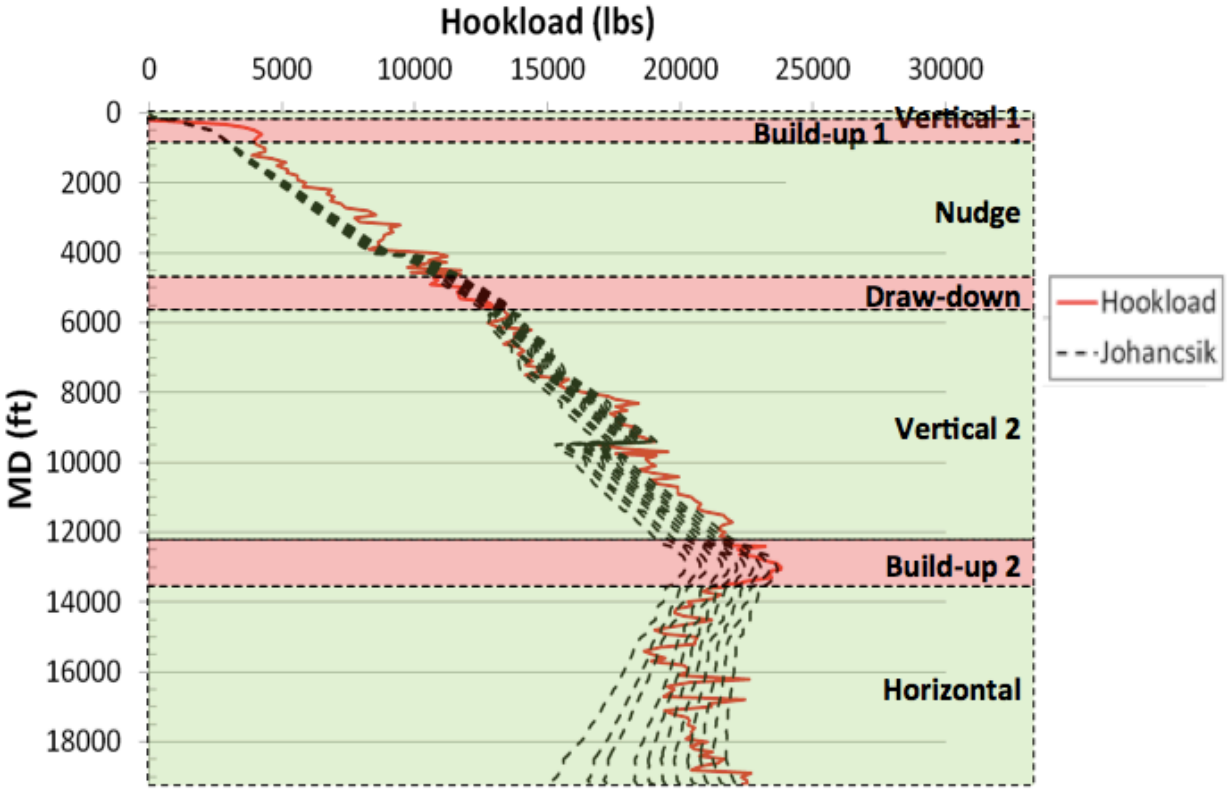

Figure 28: Dataset 2 Drag Friction Analyses by Geometry

It should be noted that a proper analysis could not be run on Vertical 1 due to its short length. Vertical 1 was described by only two data points in Dataset 3, so proper interpolations and comparisons could not be made.

After Vertical 1 has been disregarded, it can be seen in Table 23 that Johancsik's model predicts no drag friction losses in the Build-up 1 and Downward Slant, very high friction losses in Drawdown, and slightly lower friction losses in Vertical 2 and Build-up 2, and typical losses in Horizontal.

The fact that the model estimates zero drag friction losses in Build-up 1 and Downward Slant and also expresses large average relative difference (compared to the later friction sections) may suggest that some unknown phenomenon is affecting the well's hookload is not being captured by Johancsik's model. Unexplained phenomena can range from possible geologic or geometric effects to the driller lifting his hand off the brake handle for a second. But this error may also simply be due to variance. Build-up 1 is a smaller section made up of fewer data points. This may have led to worse correlations. And the error in Downward Slant, while larger than the error in the deeper sections, is not so large that it is far outside the expected range of error for drag friction.

Other than Build-up 1 and Downward Slant, Johancsik's model is able to accurately estimate the hookload for this well. For all of the other sections, the average relative difference never exceeded 5%.

After the drag analyses were conducted, torque analyses were then conducted on Dataset 3. The results from these analyses are shown in Table 24 and Figure 29 below.

Table 24: Dataset 3 Torque Friction Analysis by Geometry			
Geometry	Optimal Friction Coefficient	Average Absolute Difference (ft-lbs)	Average Relative Difference
Vertical 1*	*	0	0.0000
Build-up 1	0	253	0.9793
Downward Slant **	0.23	505	0.1282
Vertical 2**	0.29	1527	0.6610
Build-up 2	0.33	3325	1.5491
Horizontal	0.25	1617	0.9171

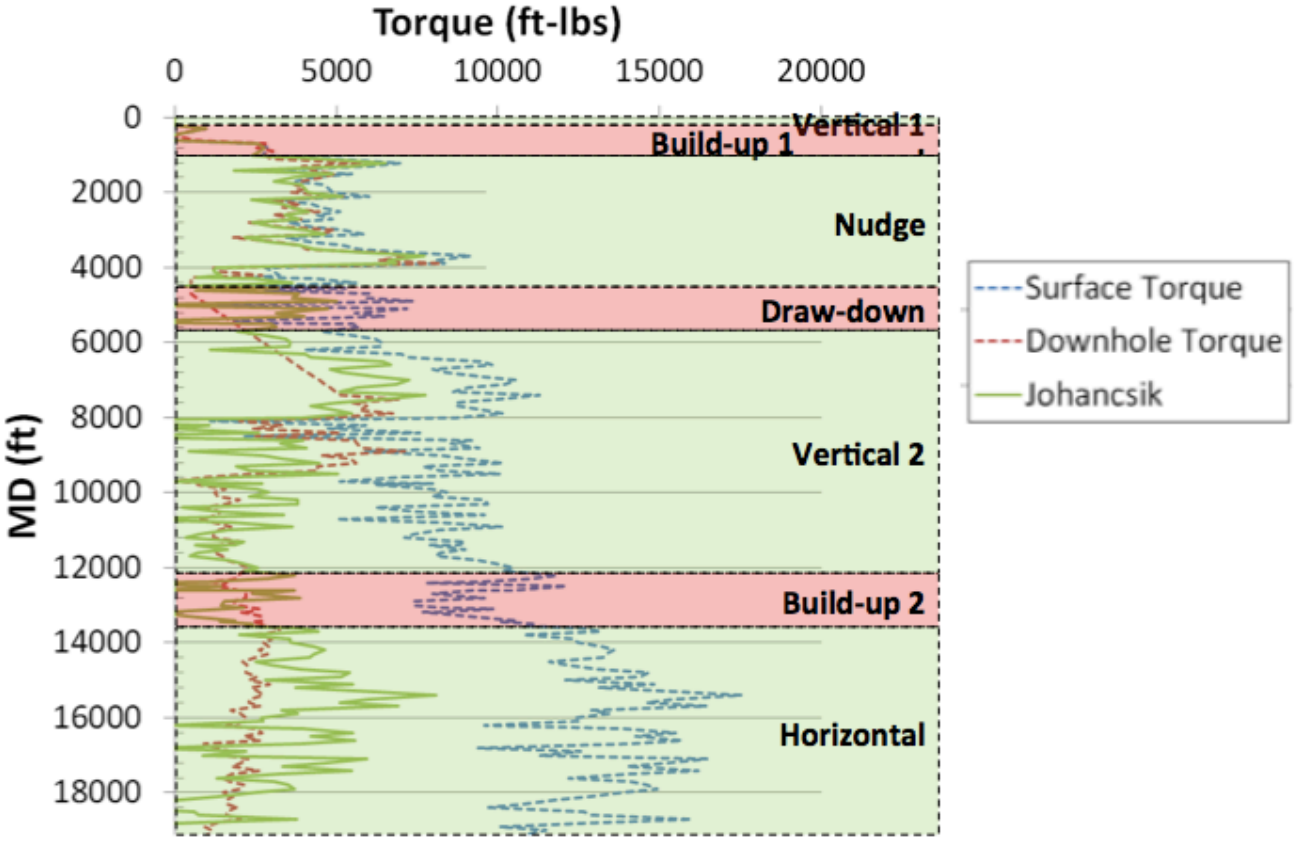

Figure 29: Dataset 2 Torque Friction Analyses by Geometry

Again, from Figure 29, it can be seen that the MWD tool malfunctioned from 4136 to 7631 ft md. This section coincides with the very end of Downward Slant, the

entirety of Draw-down, and about a third of Vertical 2. Because there is no data with which to compare Johancsik's model to, analyses could not be conducted over this interval.

Like the drag analysis, Johancsik's model predicts that Build-up 1 experiences no torque friction losses. This may be due to variance, as this is a small section with few data points or because of unexplained phenomena that is not accounted for in Johancsik's model.

Upon examining Table 24, it can be seen that the model estimates a slightly higher torque friction factor for Build-up 2 than for the straight sections (Downward Slant, Vertical 2, and Horizontal). Johancsik's model estimates that Downward Slant has the smallest torque friction loss of the wellbore, followed by a slightly greater torque loss in Vertical 2, and an in-between torque loss for Horizontal. It should be noted, however, that the straight sections tended to have friction coefficients that were about the same value while Build-up 2 had a slightly higher torque friction coefficient than even the highest straight section.

From Figure 29, it can be seen that, while Johancsik's model was able to follow the general trend of the downhole torque measurements, it did so with a lot of variance in its estimates. This is due to the large amount of variance in the surface measurements.

CHAPTER 4: DISCUSSION

Once the results from Chapter 3 have been combined, some patterns (and lack of patterns) begin to emerge. In this chapter, the effects of formation and drill string geometry on torque and drag are discussed. First, the overall results of geology are discussed, followed by the results of specific drill string geometries, and then finally an analysis of general drill string geometries.

The accuracy of the model was determined by a threshold of 0.07 average absolute differences between the calculated and average friction factor. Any average absolute difference for a formation greater than 0.07 was determined as not being captured by the model. Any average absolute difference less than 0.07 was determined to have been accurately portrayed by the model.

Torque and Drag Analysis of Overall Geologic Effects

After the results for all three data sets have been combined, they can be divided by formation. First the drag analyses will be discussed, followed by a discussion of the torque analyses. The overall drag results the results shown in Figures 30, 31, and 32 below.

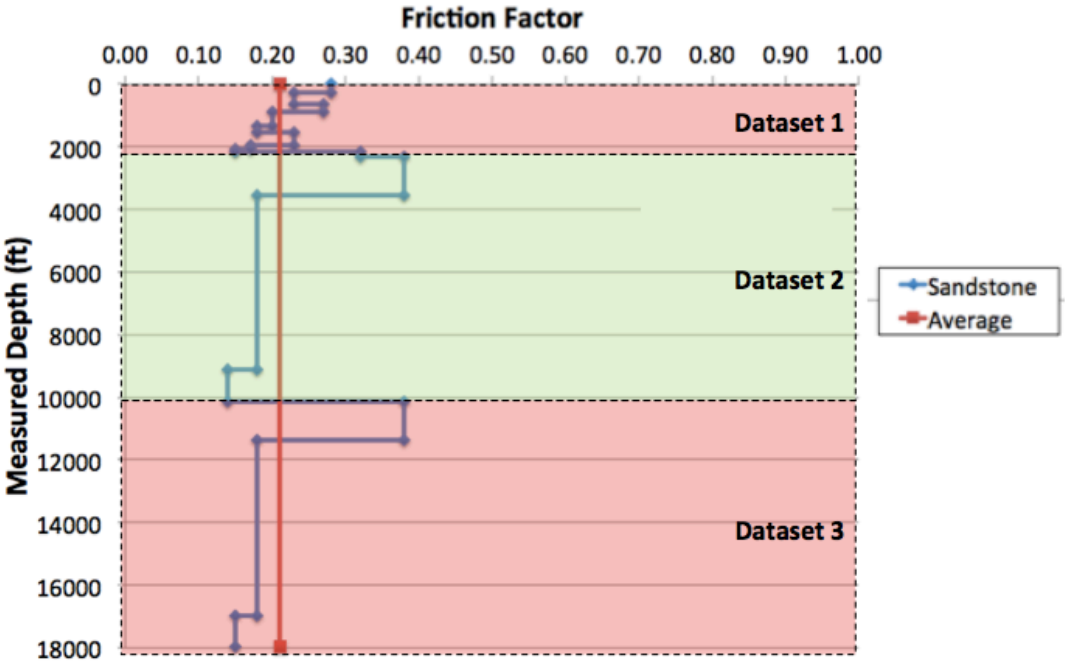

Figure 30: Drag Friction Factors for Sandstone Formations

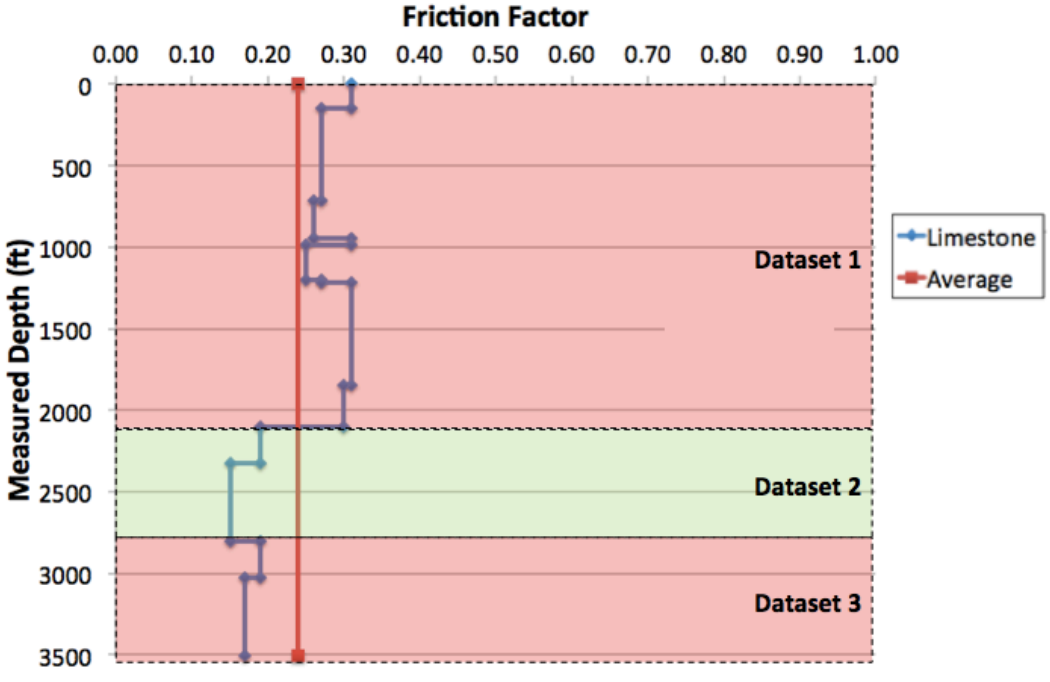

Figure 31: Drag Friction Factors for Limestone Formations

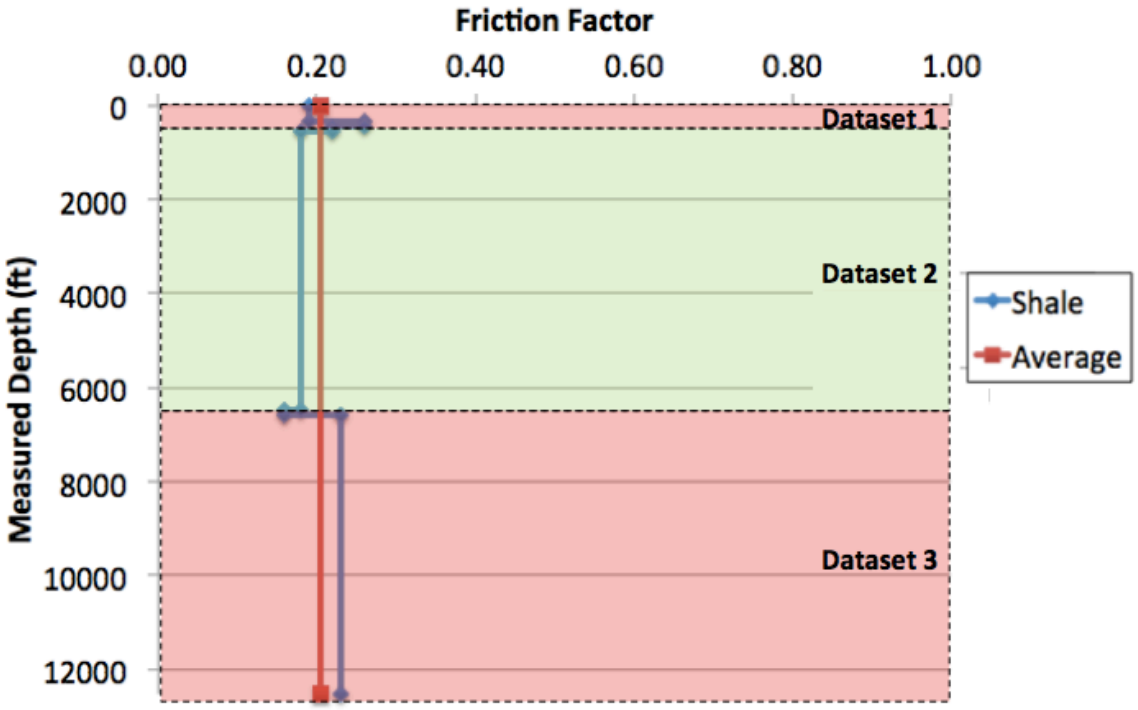

Figure 32: Drag Friction Factors for Shale Formations

These results are summed in Table 25 below.

Table 25: Summary of Overall Drag Friction Factors by Lithology			
Formation	Average Friction Factor	Average Absolute Difference	Average Relative Difference
Sandstone	0.210	0.0540	0.2571
Limestone	0.239	0.0559	0.2334
Shale	0.205	0.0251	0.1224

From Table 25, it appears that lithology has a small effect on the drag friction factor. On average, limestone formations tended to have a slightly higher friction factor than both sandstone and shale formations. Sandstone and shale formations tended, on average, to have similar friction factors. Of course, it is interesting to note that the shale formations tended to be dominated by the large horizontal sections of Dataset 2 and

Dataset 3. But despite this, the other shale sections did not deviate from these values much. Overall, it appears that lithology has a slight effect on drag friction factors and need to be accounted for in the model.

Lithology also appears to have an affect on torque friction factors, as shown in Figures 33, 34, and 35 below.

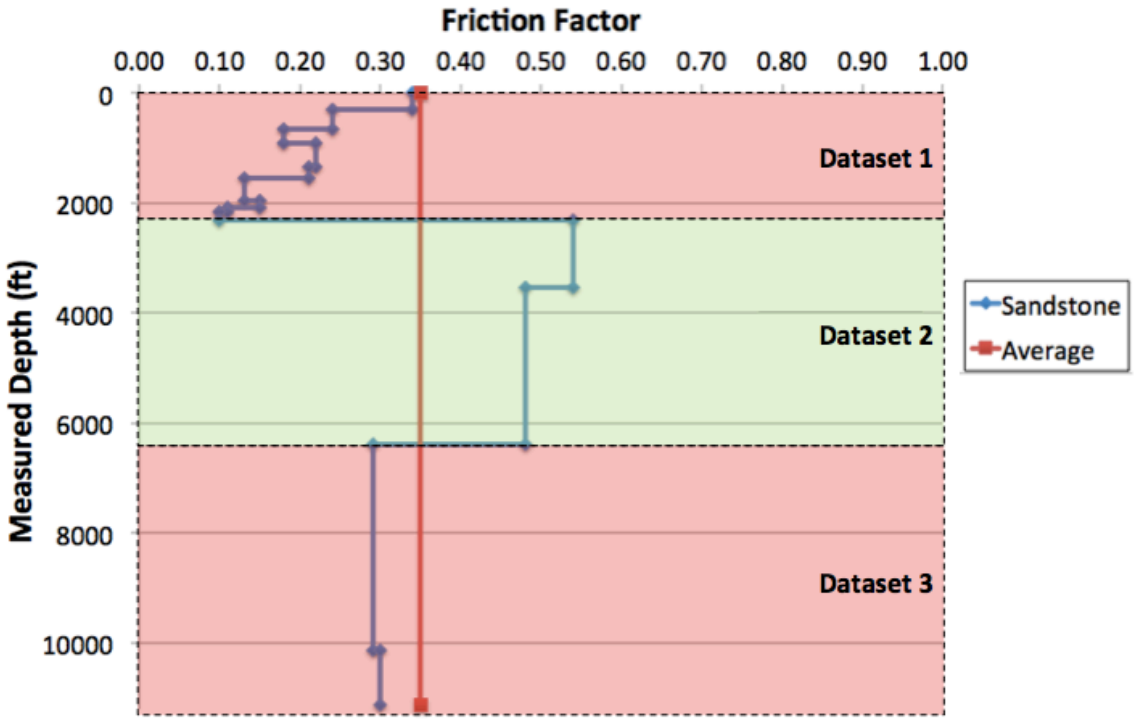

Figure 33: Torque Friction Factors for Sandstone Formations

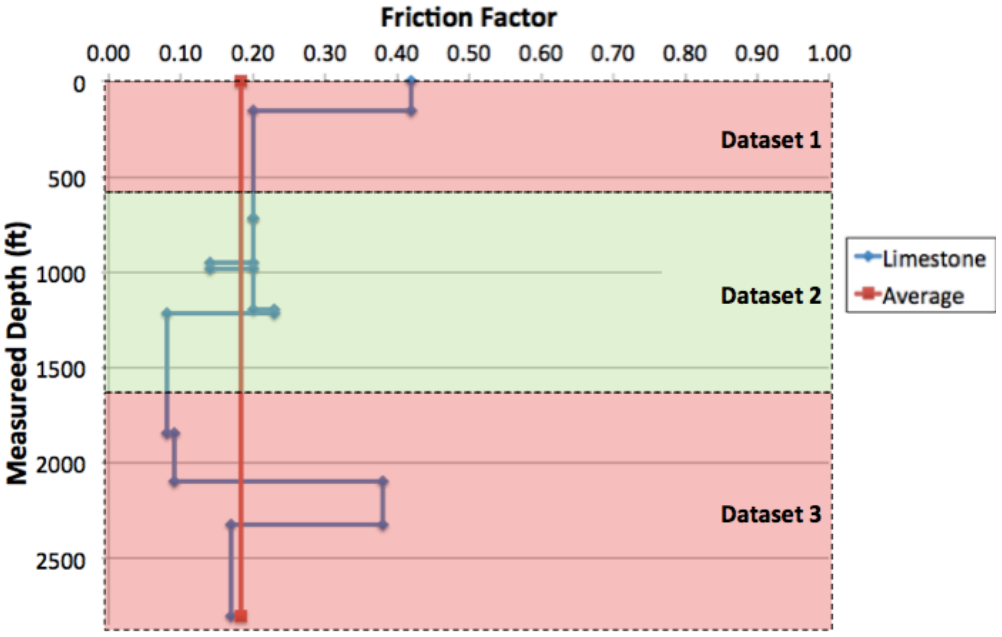

Figure 34: Torque Friction Factors for Limestone Formations

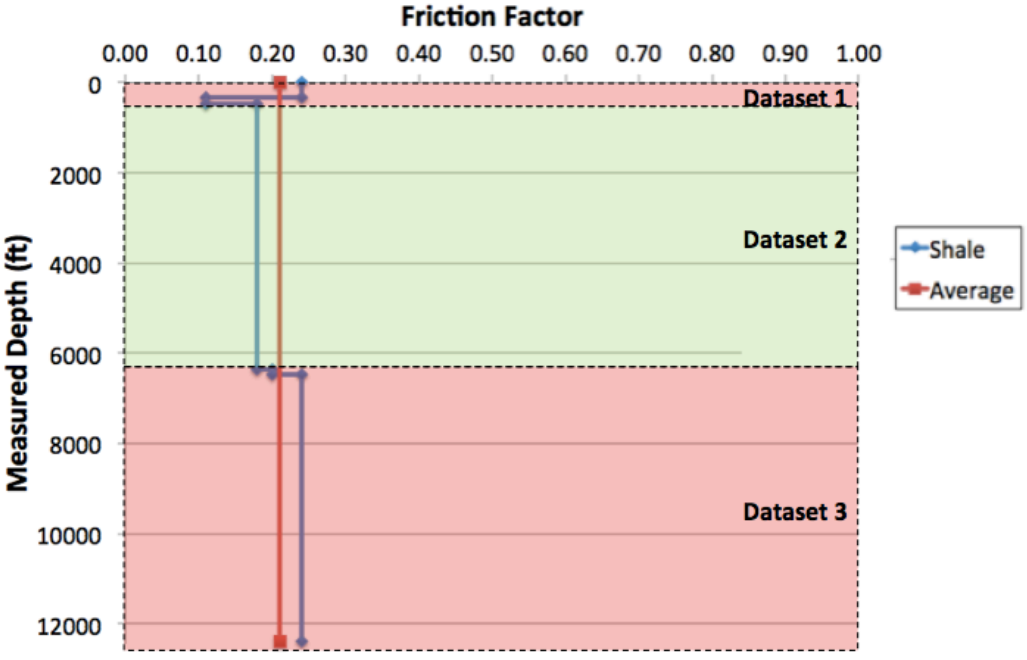

Figure 35: Torque Friction Factors for Shale Formations

The results for these figures are summarized in Table 26 below.

Table 26: Summary of Torque Friction Factors by Lithology			
Formation	Average Friction Factor	Average Absolute Difference	Average Relative Difference
Sandstone	0.349	0.1095	0.3136
Limestone	0.183	0.0693	0.3777
Shale	0.210	0.0305	0.1453

From Table 26, it can be seen that sandstones tend to have the largest average friction factor, mostly due to the high friction factors in Dataset 2. Limestone friction factors tended to be very low on average. Because the average was so low, the average relative difference tended to be high despite the absolute difference tending to be low. Shale formation's torque friction factors tended to be slightly higher than limestone torque friction factors but significantly lower than sandstone torque friction factors. Shale torque friction factors tend to be more stable than both sandstone and limestone formations. This is evidenced by the low average absolute difference and low average relative difference between the average friction factor and calculated friction factors. This is partially because the long horizontal sections dominate the shale measurements, though the friction factors of the other sections do not deviate far from the average.

The limestone torque friction factors barely meet the accuracy requirement of having an average absolute difference of less than 0.07. The absolute average differences between the sandstone friction factors, however, are significantly higher and suggest that sandstones are not modeled well. It is my opinion, however, that the large average absolute differences may be explained by drilling operations rather than failures in the

model. It was while drilling in the middle of the sandstone section that the drilling operation began to experience issues with their MWD tools. Eventually, the MWD tool failed. The high friction factors may have been caused by faulty downhole measurements some time before the downhole tool actually failed.

Torque and Drag Analysis of Overall Geometric Effects

Compiling the torque and drag results for wellbore geometry allows for a similar analysis. The results of these compilations are shown in Figures 36, 37, 38, 39, and 40, and then summarized in Table 27 below.

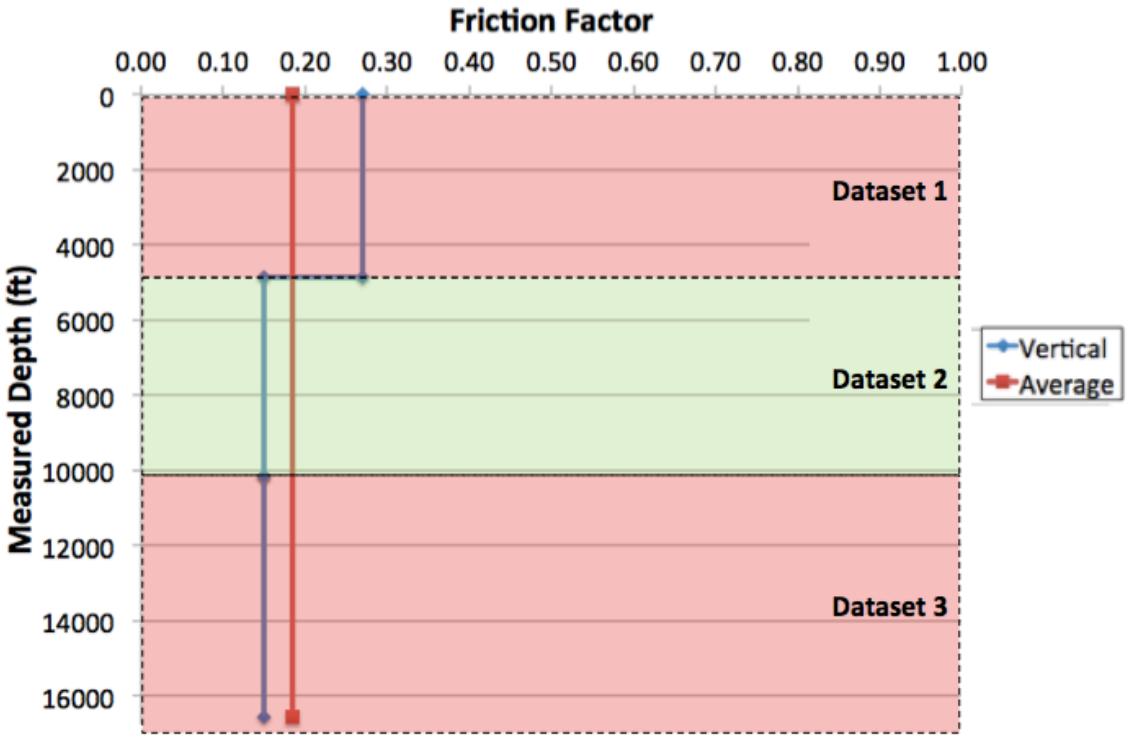

Figure 36: Overall Drag Friction Factor for Vertical Sections

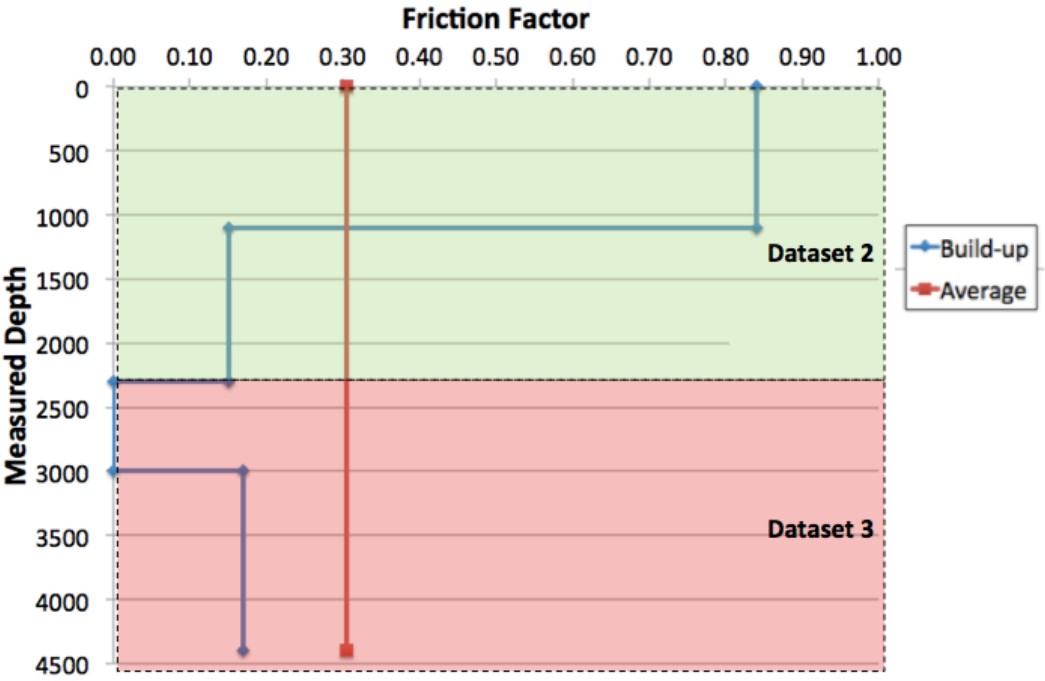

Figure 37: Drag Friction Factor for Build-up Sections

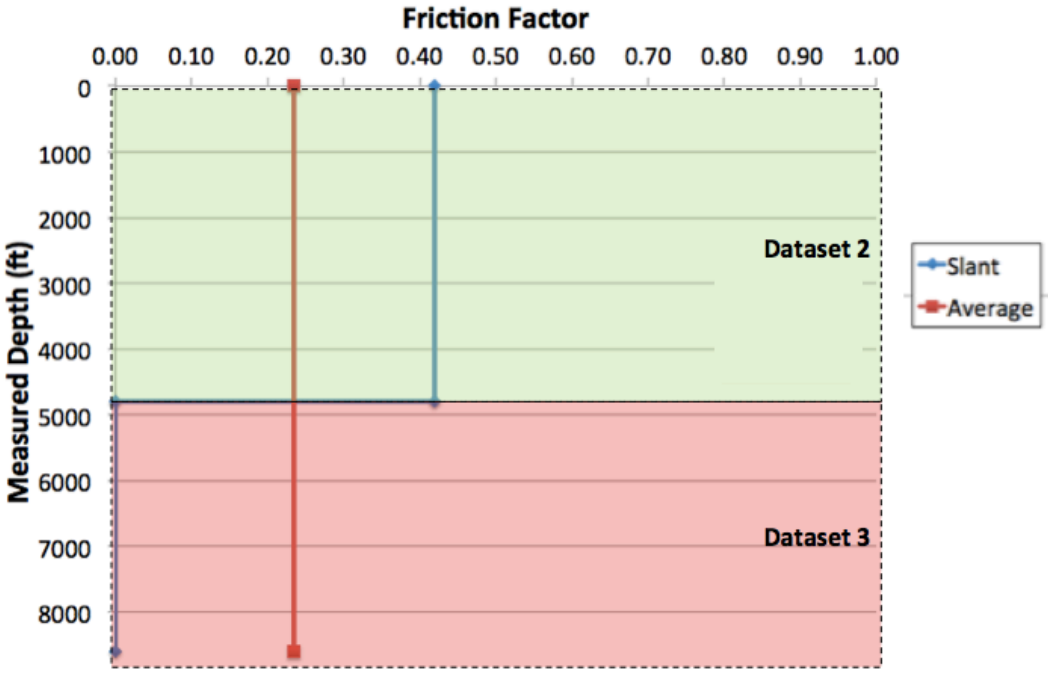

Figure 38: Drag Friction Factors for Slant Sections

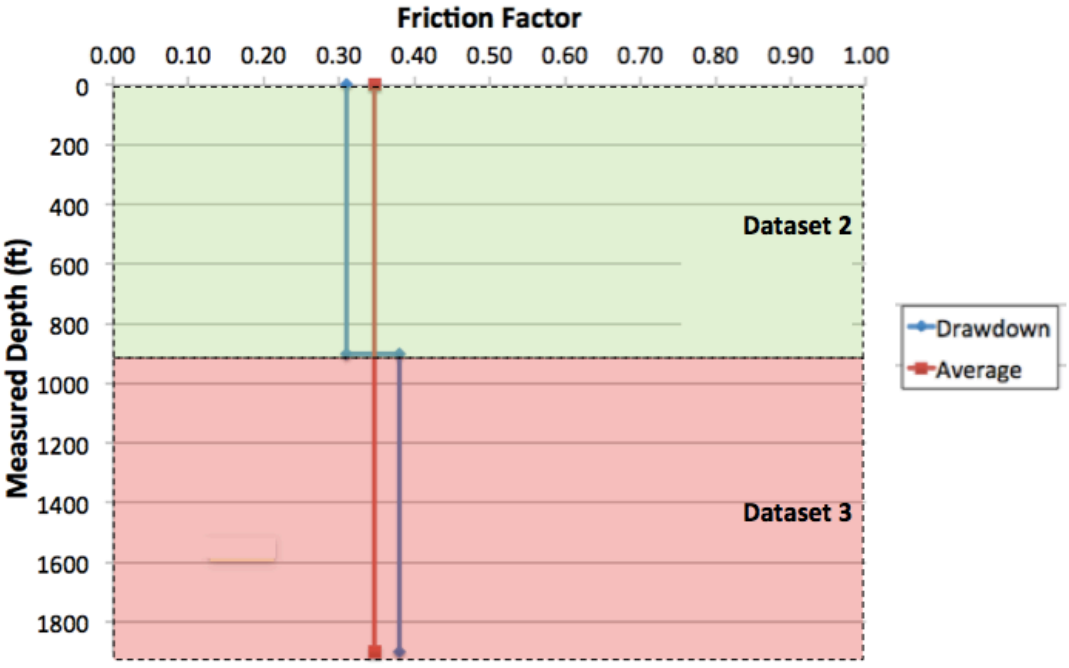

Figure 39: Drag Friction Factor for Drawdown Sections

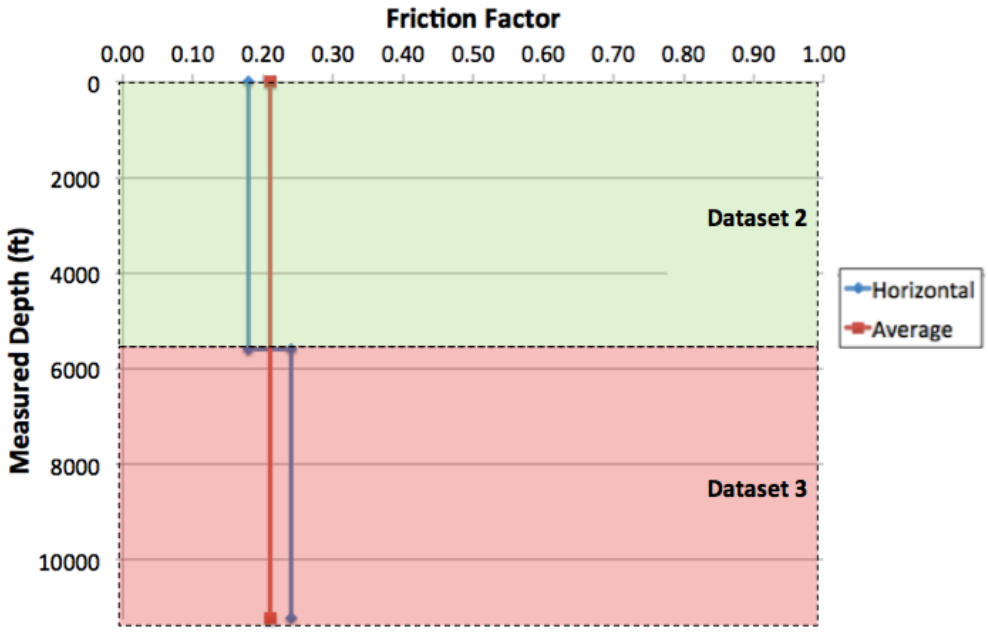

Figure 40: Drag Friction Factor for Horizontal Sections

Table 27: Summary of Drag Friction Factors by Geometry			
Trajectory	Average Friction Factor	Average Absolute Difference	Average Relative Difference
Vertical	0.185	0.050	0.2689
Build-up	0.305	0.268	0.8770
Slant	0.234	0.207	0.8837
Drawdown	0.347	0.035	0.1006
Horizontal	0.210	0.030	0.1428

Two noticeable facts stand out from the figures and table. First, many sections do not have large sample sizes (most sections had only two data points to draw analyses from). Second, it seems that the model accurately analyses the vertical, drawdown, and horizontal sections and does not properly estimate the friction losses for the build-up and slant sections. But again, it should be stressed that the sample sizes for these sections is small.

This issue was even worse when compiling torque friction factors due to the failure of the downhole tools. The results of the torque friction factors for specific trajectories are shown in Figures 41, 42, 43, 44, and 45 and Table 28 below.

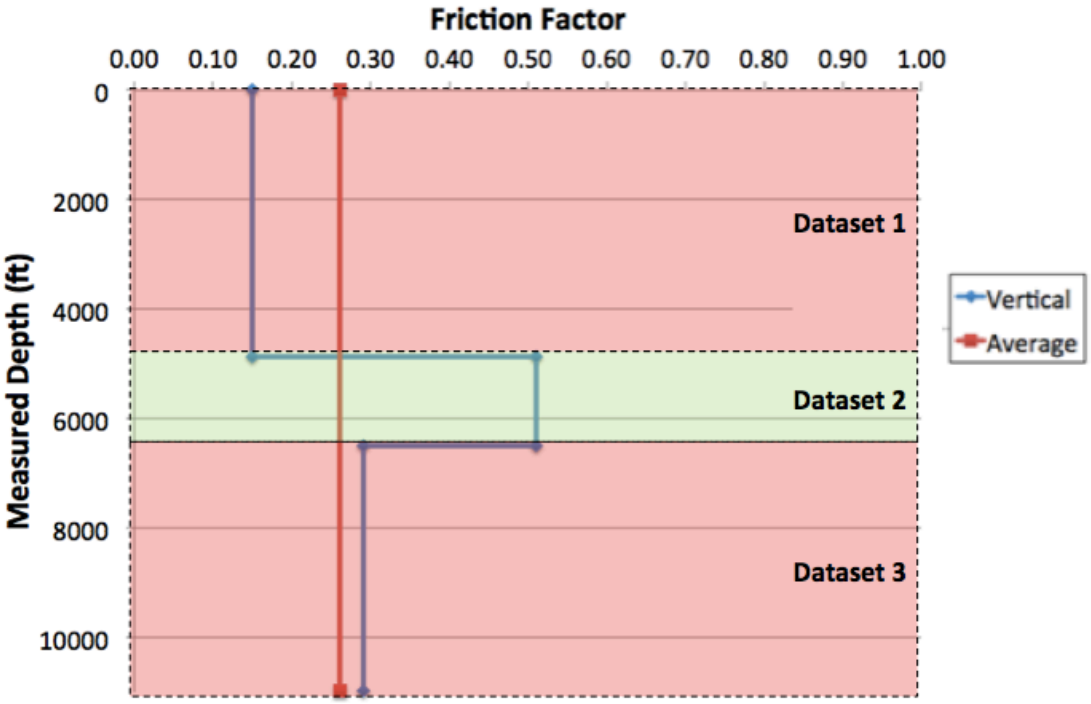

Figure 41: Torque Friction Factors for Vertical Sections

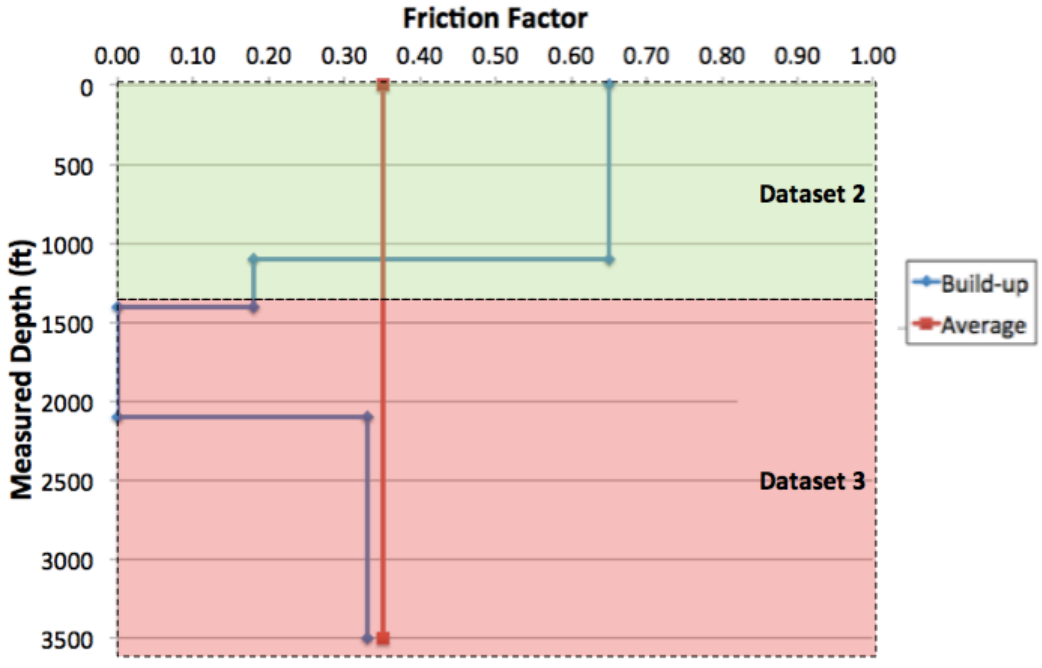

Figure 42: Torque Friction Factors for Build-up Sections

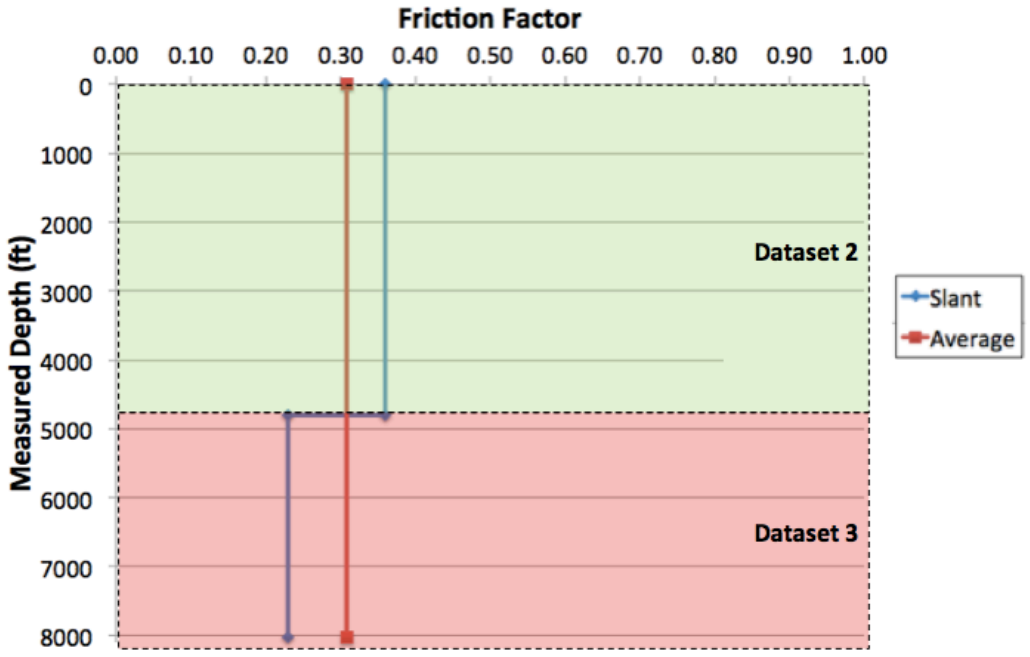

Figure 43: Torque Friction Factor for Slant Sections

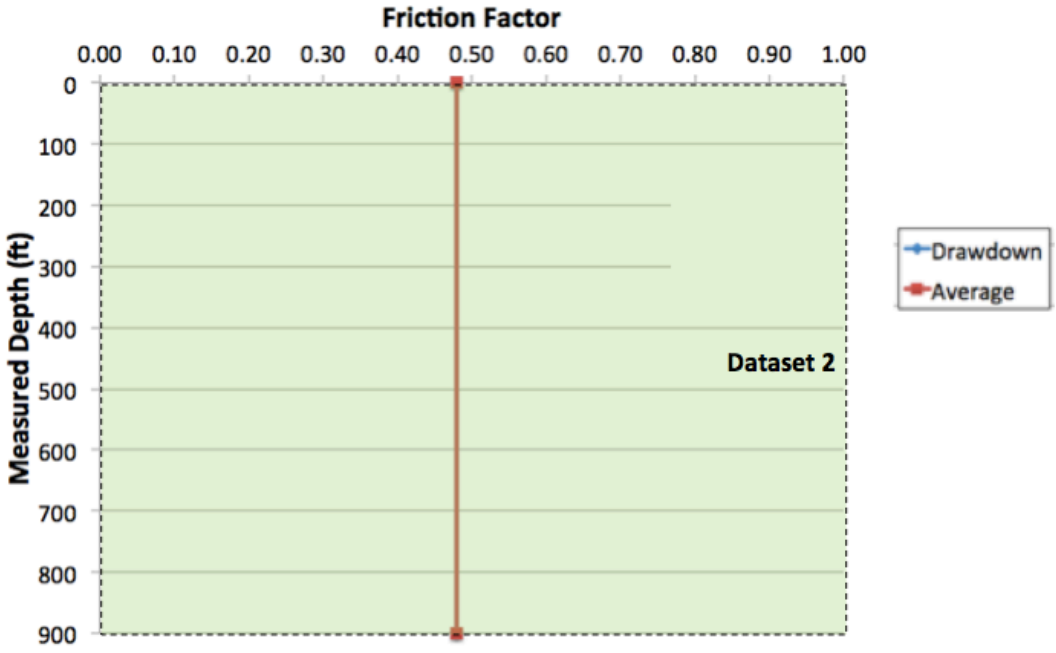

Figure 44: Torque Friction Factor for Drawdown Sections

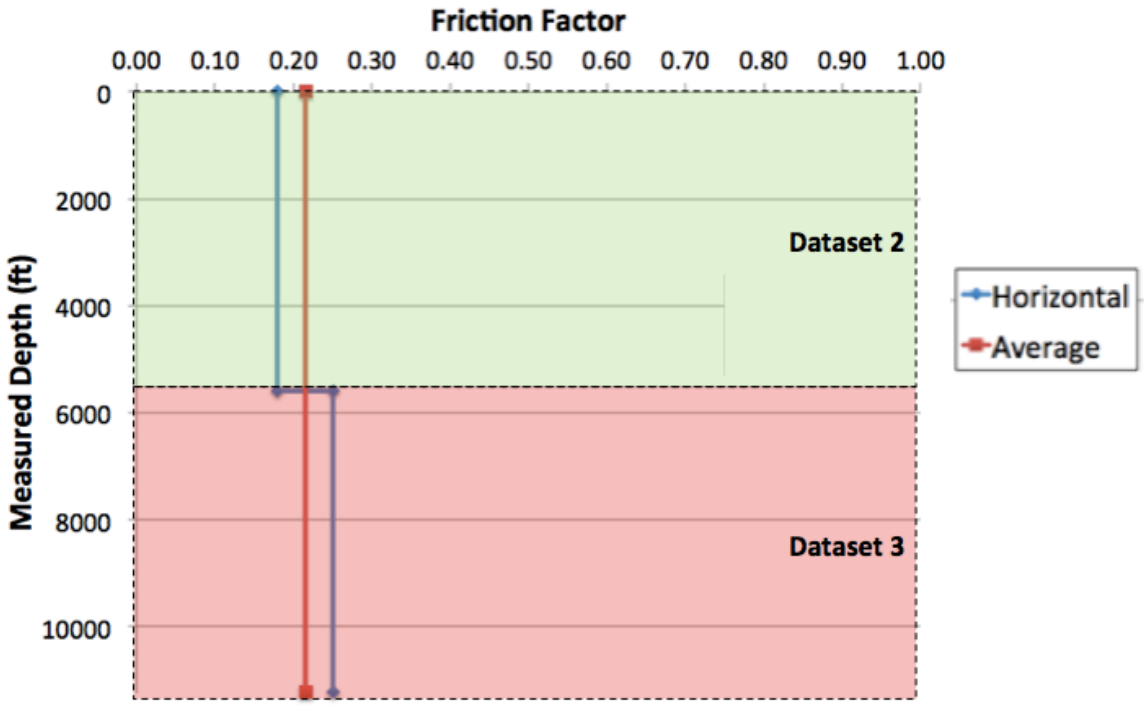

Figure 45: Torque Friction Factors for Horizontal Sections

Table 28: Summary of Torque Friction Factors by Geometry			
Trajectory	Average Friction Factor	Average Absolute Difference	Average Relative Difference
Vertical	0.261	0.098	0.3777
Build-up	0.352	0.187	0.5331
Slant	0.308	0.063	0.2033
Drawdown	0.480	0	0
Horizontal	0.215	0.035	0.163

From the above figures and table, it can be seen that, while it appears the model is able to fairly accurately predict the torque friction factors by geometric section, it may not necessarily be able to due to the small sample sizes of the sections. The sections

contain even fewer data points than the drag sections due to the difficulties experienced with the downhole tools.

In order to solve the sample size issue, the above analyses were consolidated further. The results of straight sections and curved were compared. The drag friction factors are shown in Figures 46 and 47 and summarized in Table 29 below.

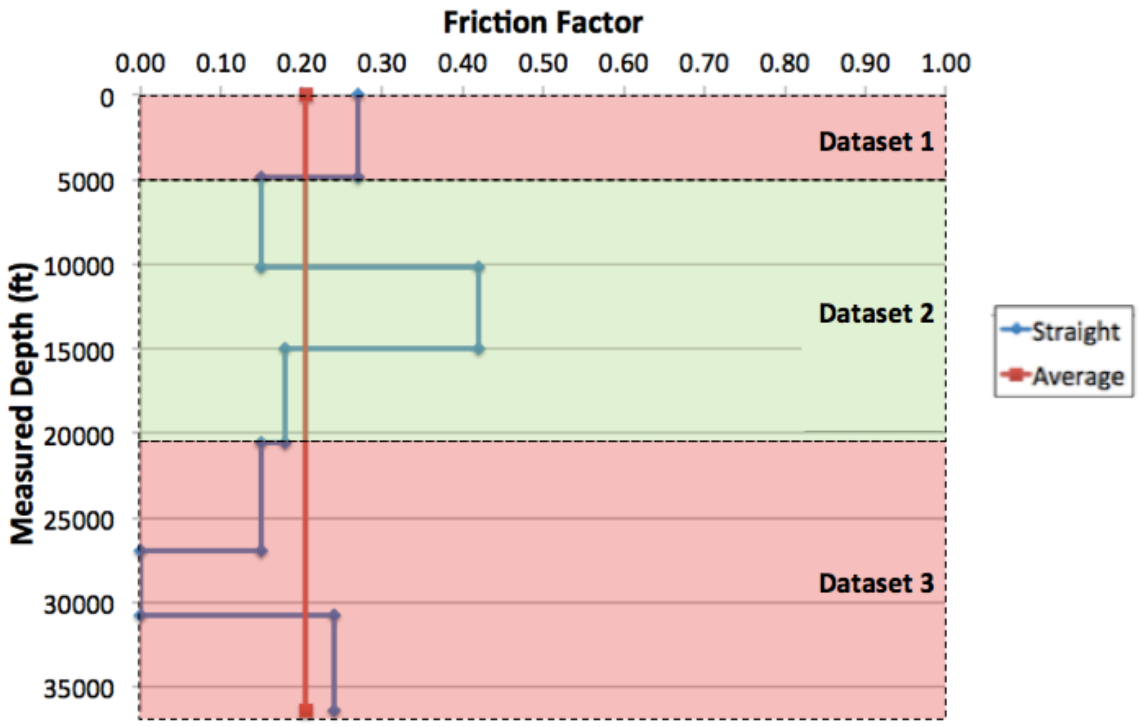

Figure 46: Drag Friction Factors for Straight Sections

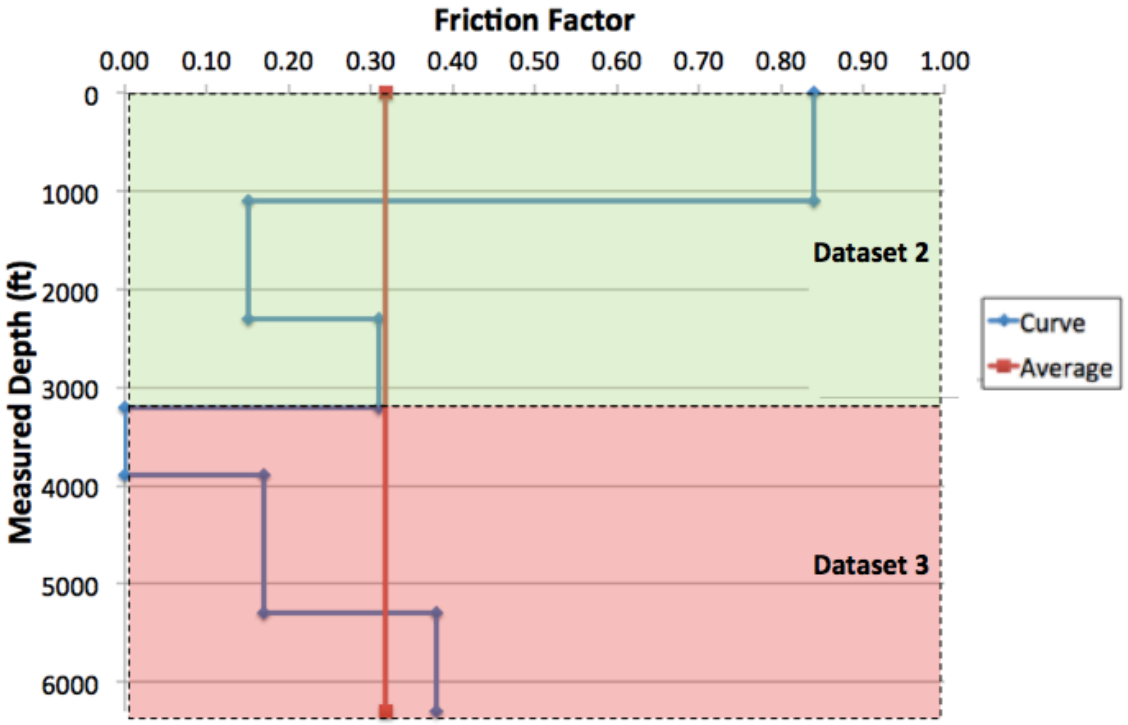

Figure 47: Drag Friction Factors for Curved Sections

Table 29: Summary of Drag Friction Factors by Geometry			
Trajectory	Average Friction Factor	Average Absolute Difference	Average Relative Difference
Straight	0.205	0.085	0.4172
Curved	0.318	0.202	0.6367

From the above tables and figures, it appears that the model is not good at distinguishing between straight segments and curves. A general friction coefficient was not able to be determined for either geometry. This makes sense, however, as the segments included in these sections include segments with very different inclinations and changes in inclinations (vertical, slanted, and horizontal segments were included in the

Straight analysis, while build-up and drawdown segments were included in the Curve analysis).

Compiling the torque analyses on straight and curve segments proved no more useful than the drag analysis. The results of the torque compilations are shown in Figures 48 and 49 and Table 30 below.

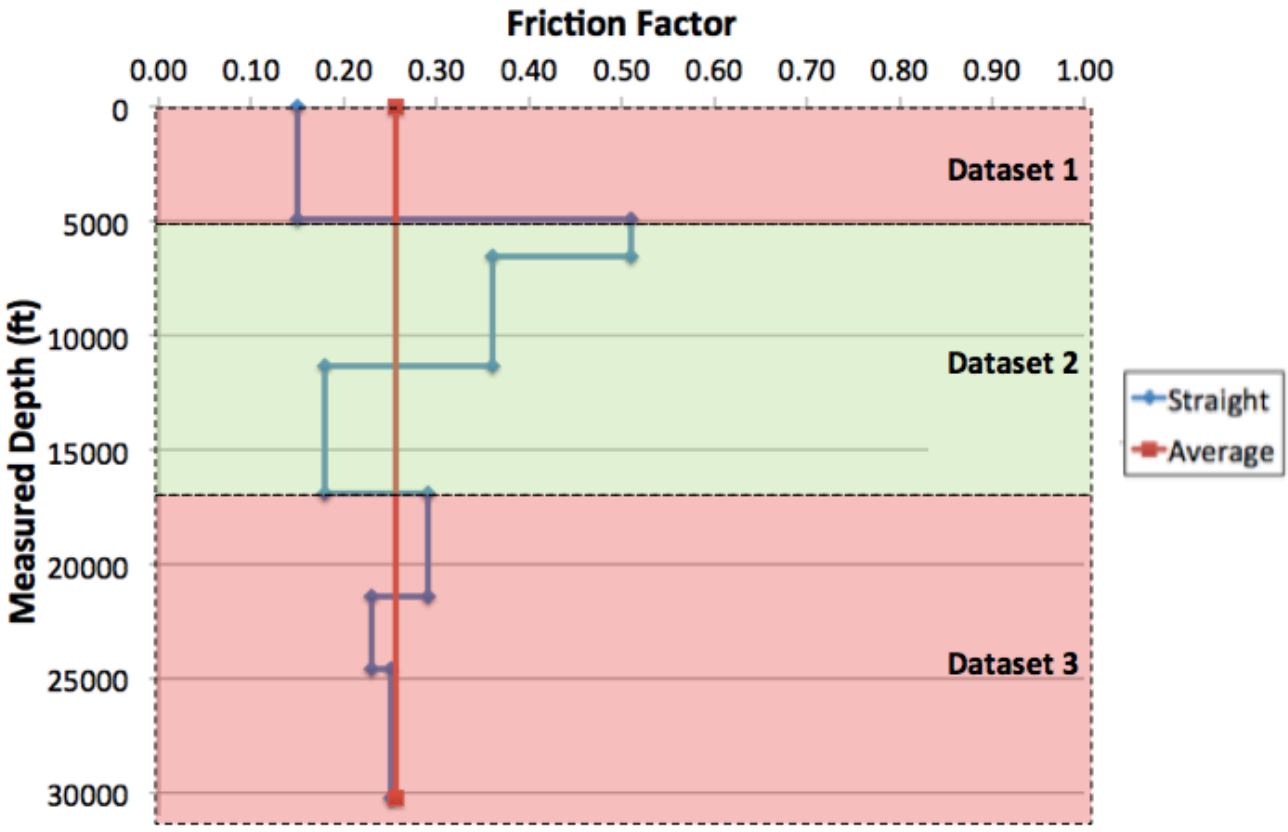

Figure 48: Torque Friction Factors for Straight Sections

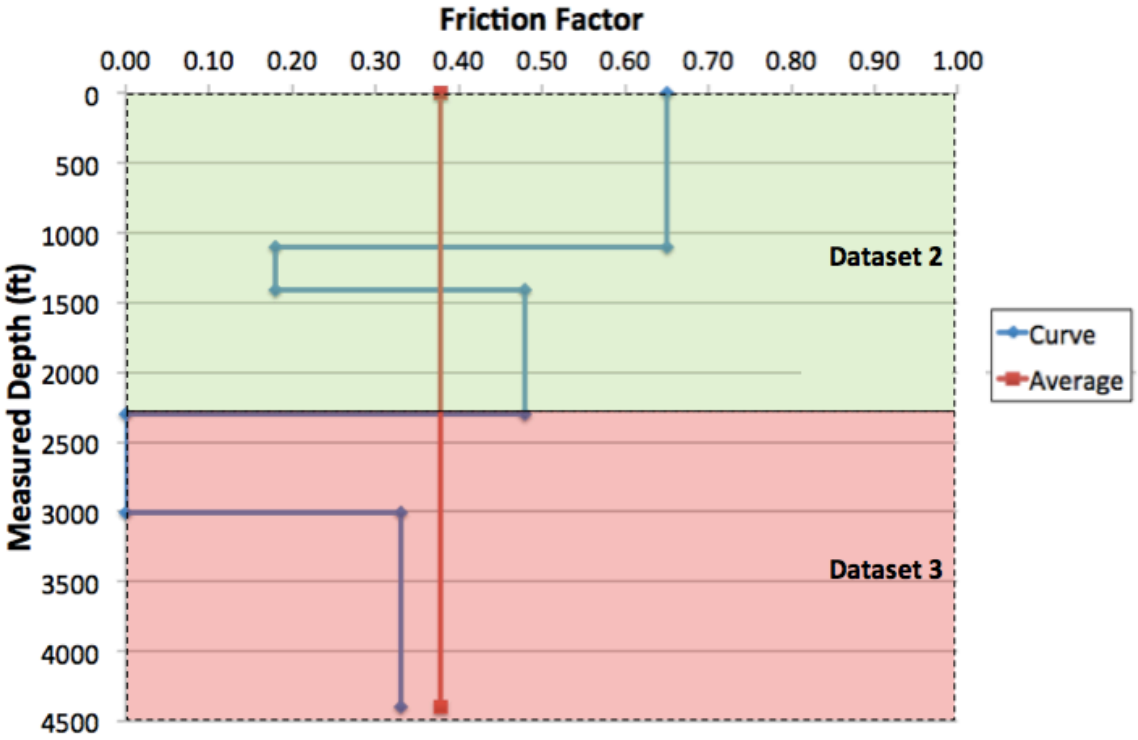

Figure 49: Torque Friction Factors for Curved Sections

Table 30: Summary of Torque Friction Factors by Geometry			
Trajectory	Average Friction Factor	Average Absolute Difference	Average Relative Difference
Straight	0.256	0.070	0.2747
Curved	0.378	0.178	0.4704

From the above figures and table, it is easy to see that the model was unable to find a single friction factor to describe straight and curved sections. Again, this can be attributed to several factors, including the breadth of geometries included in "straight" sections and "curved" sections. And even though the straight sections, according to Table 30, appear to be estimated by a 0.256 friction factor, it can be seen from Figure 49 that the low average differences are due to the relatively unchanging torque friction factor in Dataset 3. The torque friction differences in Dataset 1 and Dataset 2 are much more

erratic, which suggests that the simply examining “straight” sections and “curve” sections is not specific enough to estimate accurate torque friction factors.

Overall, when examining wellbore geometry’s torque and drag friction effects, it is not enough to simply examine “straight” sections and “curved” sections. The geometric effects are much more subtle than such a simplification. It is possible that torque and drag effects of more specific geometries (such as build-up, drawdown, and slant sections), but given a lack of data, proper conclusions could not be reached.

CHAPTER 5: CONCLUSIONS AND FUTURE WORK

Overall, the results of this thesis were mixed. There are suggestions that geologic effects definably and there are suggestions that specific geometric effects may affect torque and drag calculations, but given the lack of volume of data, it is hard to conclude anything definitively. More analyses need to be conducted before more clear patterns can emerge. But rather than define these effects by itself, this thesis should be a stepping-stone that contributes to a more comprehensive future work that will explore these effects.

There are several directions from which to take this project. The most obvious direction is to conduct more analyses using more data. This is especially true for examining the geometric effects on torque and drag. Much more data from specific wellbore geometries is needed so that proper comparisons can be made. Ideally, at least ten data points would be analyzed to give an idea of some sort of trend and any outliers.

Other than further and better analysis, however, there are some more interesting places to further development. The first is application of downhole torque modeling to Mechanic Specific Energy (MSE) models. It is widely stated that the largest sources of inaccuracy in mechanic specific energy models are the torque terms (Teale 1965). The torque terms in these models do not properly account for the friction losses along the drill string during drilling operations. By accounting for friction losses, the MSE models should be theoretically more accurate.

Another direction to take this project would be to expand upon the MSE applications further and design an automated drilling system that would conduct a drilling operation under particular inputs (WOB and RPM), calculate MSE from the resulting outputs and modeled torque, and then adjust the WOB and RPM to result in a lower MSE. This would theoretically result in a more efficient drilling operation and extend tool life and decrease NPT.

These three directions are discussed in further detail below.

Conducting Further Analyses

Due to lack of data, the analyses conducted on specific drill string geometries remained inconclusive. No geometry contained more than four data points and one geometry contained only one data point. This is not enough data to draw any conclusions from. To draw a proper conclusion, at least ten data points in each section are required, though to produce any sort of statistically significant value, even ten is not enough. Realistically, however, an analysis on ten different wells should provide enough data to get good comparisons

Application to Mechanic Specific Energy Models

MSE models estimate the energy it takes to drill through a particular volume of rock (Teale 1965). They are based on the idea that two particular rocks of the same composition are placed under the same conditions, will require the exact same amount of energy to drill through. Using a variety of drilling parameters, MSE models estimate

what this energy is in order to get an idea of how efficient the current drilling operation is. The higher the MSE value, the less efficient the operation is and the more important it becomes to make rig-site changes in order to increase efficiency.

Teale's MSE model is given in Equation 3 below.

Equation 3. $$MSE = \frac{WOB}{A} + \frac{2\pi}{A}\left(\frac{NT}{\mu}\right)$$

where

MSE = Mechanic Specific Energy
WOB = Weight-on-bit
A = The area of the hole section being drilled
N = Rotation speed (rpm)
T = Torque
μ = Penetration rate

From Equation 3, we see that one of the principle parameters in Teale's MSE model is torque. Furthermore, torque is a principle component of almost all MSE models. Pessier (1992), Dupriest (2005), Armenta (2008), Mohan (2009), and Rashidi (2010) are just a handful of the MSE models that depend on torque values as a key component.

It is also the source of greatest error within the model. Whereas the other parameters in Equation 1 are easily measured, there are discrepancies as to the accuracy of the torque measurements. Using surface torque measurements is questionable because of the downhole friction losses experienced during drilling operations. These friction losses are not captured in the model if using surface torque measurements. It is therefore important to either measure downhole torque measurements from an MWD tool or to estimate downhole torque. By using downhole torque measurements, the MSE value

should be much more accurate, allowing for a more accurate portrayal of drilling efficiency to be conducted.

Automated Drilling Systems

Once MSE can be calculated quickly and accurately, it can be used to develop an automated drilling system. This system would use weight-on-bit (WOB) and rotary speed (RPM) as system inputs and then, during drilling operations, measure drilling parameters. These parameters would then be used to calculate downhole torque (using a downhole torque and drag model) and MSE. The system would then vary WOB and RPM slightly to see how MSE changes and then attempt to find the system with the lowest MSE to maximize drilling efficiency. A diagram of this process can be found in Figure 50 below.

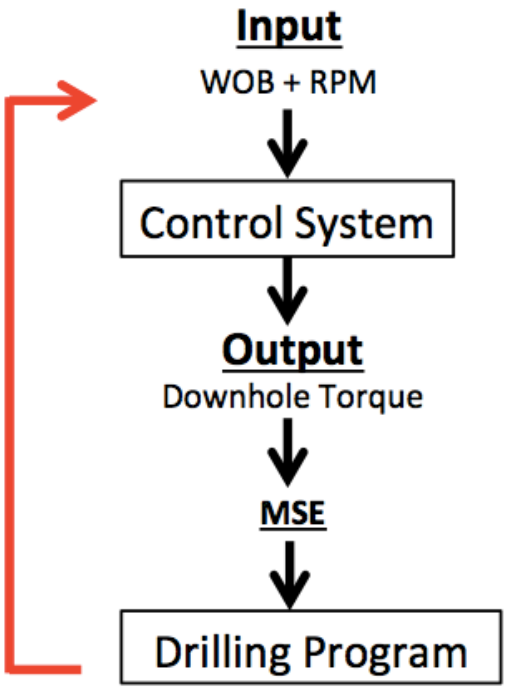

Figure 50: Schematic of Automated Drilling Program

From Figure 1, we see that the drilling schematic creates a feedback loop, where the inputs enter the system, output downhole torque, which is then input along with other drilling parameters into a MSE model, which is then used to find more optimal input values. This feedback loop will should generate a system that will minimize MSE and hence maximize drilling efficiency. This will lead to increased tool life and decrease NPT.

APPENDIX A—JOHANCSIK'S TORQUE AND DRAG MODEL

In 1984, Johancsik et al (1984) developed the model to estimate the downhole friction losses experienced during drilling operations. Its main purpose was to help with well planning and drill string design. The model uses a finite element approach to estimate the loads acting on the drill string and to estimate the losses. The model first divides the drill string into several elements and looks at the loads acting upon each individual element. An example of an element and its loads can be seen in Figure 51 below.

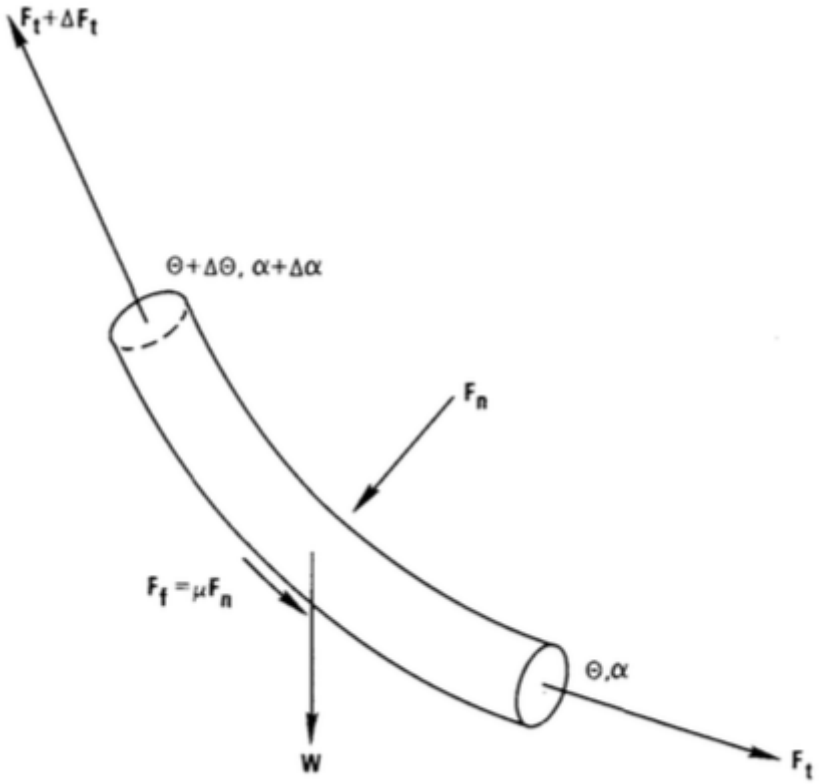

Figure 51: Drill String Element and Loads (Johancsik et al. 1984)

where, in the above figure,

F_n = normal force
F_t = drill string tension
ΔF_t = change in drill string tension along drill string element
Θ = inclination
$\Delta\Theta$ = change in inclination along drill string element
α = azimuth
$\Delta\alpha$ = change in azimuth along drill string element
W = buoyed weight of drill string element
F_f = friction force
μ = coefficient of friction

Loads Acting upon Drill String Element

As can be seen in Figure 1, there are five main forces acting upon each element—the string weight of the element, the normal force acting upon the element, the axial friction loss acting against the motion of the element, and the tension forces acting at both ends of the element.

STRING WEIGHT

The string weight is the pipe weight buoyed by drilling fluids. It is equal to the dry weight of the element (found from drill string specifications) multiplied by the buoyancy factor. The buoyancy factor is the fraction of drill string that is not displaced by the drilling fluids and is found by subtracting the ratio of drilling fluid and steel densities from 1. These can be found in Equations 4 and 5 below.

Equation 4. $W_b = \beta W$

Equation 5. $\beta = 1 - \frac{\rho_f}{\rho_{steel}}$

where

W_b = buoyed drill string weight
W= dry drill string weight
β= buoyancy factor
ρ_f= drilling fluid density
ρ_{steel}= steel density

NORMAL FORCE

The normal force is the contact force between the element and the wellbore. It has two main components—the weight of the drill string and the tension acing through the curvature of the drill string. The drill string weight is the buoyed weight calculated above. The tension acting through the curve is based on the minimum curvature method of drill string interpolation. Johancsik et al. considered that there may be other forces that contribute to the normal force, such as pipe bending, but they considered these contributions negligible. The formula for the normal force can be estimated using Equation 6 below.

Equation 6. $F_n = \sqrt{(F_t \Delta\alpha \, sin\theta)^2 + (F_t \Delta\theta + W_b sin\theta)^2}$

where

F_n= normal force
F_t= drill string tension at *bottom* of element
$\Delta\alpha$= change in azimuth in element
θ= inclination of *bottom* of element
$\Delta\theta$= change in inclination of element
W_b= buoyed drill string weight

FRICTION LOSS

The axial friction losses are estimated by multiplying the normal force by a friction factor. This friction factor is a "lump sum" parameter that cannot be directly

calculated. How it is determined is discussed later in Appendix C. This is the loss experienced as the drill string while running drill pipe into hole or pulling drill pipe out of hole. It is the Coulomb friction loss estimate and can be seen in Equation 7 below.

Equation 7. $$F_{fric} = \mu F_n$$

where

F_{fric}= axial friction loss
μ = coefficient of friction
F_n= normal force

DRILL STRING TENSION

The drill string tension is the sum of the axial forces acting upon the drill string. Because the model uses a finite element approach, the tensions at the top and bottom of an element are considered. The tensions are continuous throughout the drill string. As such, the tension at the top of an element is equal to the tension at the bottom of the next element. The change in tension of a particular element, however, is based on the axial contribution of the buoyed drill string weight and the friction loss. This change can be seen in Equation 8 below.

Equation 8. $$\Delta F_t = W_b cos\theta \pm \mu F_n$$

where

ΔF_t= change in drill string tension in a drill string element
W_b= buoyed drill string weight
θ= inclination of *bottom* of element
μ = coefficient of friction
F_n= normal force

DRAG LOSSES

The tension at the top of the drill string is equal to the theoretical hookload of the drill string given friction losses. The total axial friction losses are the sum of the friction

losses acting upon all drill string elements. This sum is the total drag forces acting upon the drill string and are the additional loads occurred during drilling operations.

TORQUE LOSSES

The torque lost on each element is a factor of the rotating drill string contacting the well bore. This creates a torque that acts against the torque that is applied for drill operations. This loss can be calculated by multiplying the friction force and the radius of the drill string. This can be seen in Equation 9 below.

Equation 9. $$\Delta T = F_{fric} r$$

where

ΔT= torque loss in drill string element
F_{fric}= axial friction loss
r = drill string radius.

The sum of all torque losses is the total torque lost in the drill string, which is the additional amount of torque that needs to be applied in order to rotate the drill string for drilling operations. This is an important factor to estimate due to its importance at every stage of drilling procedures, from well planning to drilling operations to post-well analysis. The difference between the total torque loss and the applied surface torque is the toque that is actually applied to the drill bit.

APPENDIX B—MINIMUM CURVATURE METHOD

The minimum curvature method is a method of interpolation that is commonly used in well planning due its simplicity and its smoothness. It assumes that two points are connected by the circular curve with the smallest possible radius between these those two points. An example of the minimum curvature method can be seen in Figure 52 below.

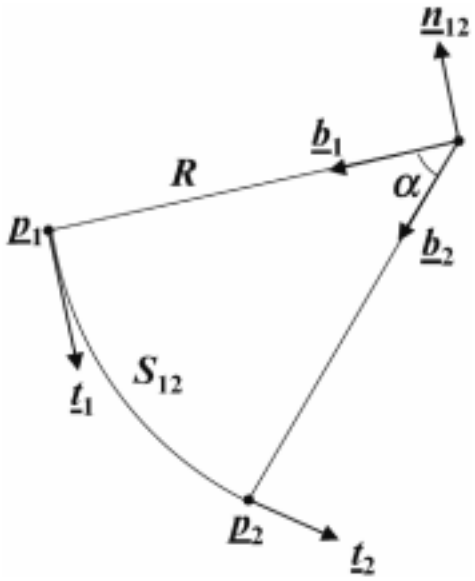

Figure 52: Example of Minimum Curvature Method (Sawaryn 2005)

where, in the above figure,

p_i = position vector of survey point i
R = radius of curvature
S_{ij} = arc length between survey points i and j
t_i = direction vector of survey point i
$\underline{b_i}$ = negative normal vector for survey point i
α = subtended angle
n_{ij} = binormal vector of survey points i and j

Example of Minimum Curvature Method

The smoothness of the minimum curvature method gives the model some semblance of being a realistic representation of the wellbore. The realism of the minimum curvature method is debatable—Mitchell and Samuel (2009) argue that because the minimum curvature method assumes a discontinuous curvature, it cannot accurately represent the wellbore. This is because a discontinuous curvature would assume that the drill string has a discontinuous bending moment, which they argued is not a realistic. But it has been argued that there is no reason that a drill string can have *cannot* have a discontinuous bending moment (Taylor and Mason 1972). Given that it is arguable that the minimum curvature method is a satisfactory representation of wellbore conditions and that the minimum curvature method is widely used throughout industry and that it was used to in Johancsik et al.'s torque and drag model, it was also used for this paper's analyses.

The minimum curvature method can be used in two ways, depending on what set of inputs is given. Inclination angles, azimuth angles, and depth drilled can be used to estimate the location of the drill bit in space, or the drill bit's location in space can be used to estimate its inclination angle and azimuth angle.

To calculate the drill bit's location from a given inclination, azimuth, and measured depth, Equations 10, 11, and 12 can be used.

Equation 10. $\Delta N = sin\theta cos\phi$

Equation 11. $\Delta E = sin\theta sin\phi$

Equation 12. $\Delta V = cos\theta$

where

ΔN = change in northing position
ΔE = change in easting position
ΔV = change in vertical position
θ = inclination angle
ϕ = azimuth angle

These calculations are fairly trivial, derived from arc length formulas in 3-D space. The second use of the minimum curvature method, however, is more involved and useful when specific points in space that the wellbore is desired to go through. To determine the change in the inclination and azimuth angles between two specific points in space, Equations 13 and 14 can be used.

Equation 13. $\Delta\theta = 2 * \sin^{-1}(\frac{d_{ij}}{2R})$

Equation 14. $\phi = \cos^{-1}\left(\frac{\left(m_{ij}^2+m_{iz}-m_{jz}^2\right)}{2m_{ij}m_{iz}}\right)$

where

$\Delta\theta$ = change in azimuth angle
ϕ = azimuth angle
d_{ij} = distance between two survey points
m_{ij} = northing and easting distance between survey points
m_{iz} = distance between survey point i and artificial point directly north of point i
m_{jz} = distance between survey point j and artificial point directly north of point i

APPENDIX C—DETERMINING FRICTION FACTOR

Johancsik's torque and drag model is based upon a Coulomb friction parameter. This friction parameter is the fraction of the applied surface torque that is acting on the drill bit. Unfortunately, however, the friction parameter cannot be directly calculated. It can only be inferred by comparing the model's output to the applied surface loads, where a "correct" friction parameter is a model output that successfully matches the surface loads. Friction parameters are iterated within the model until the correct parameter is estimated. This is most efficiently done within industry by creating "broomstick plots," which are so named because their shape resembles a broom. Broomstick plots provide a visual representation of the various model results and the surface data, allowing for results and measurements to be compared easily. They are constructed by overlaying several iterations of the model with varying friction coefficients with the surface measurements.

Example of Broomstick Plot

An example broomstick plot can be seen in Figure 53 below.

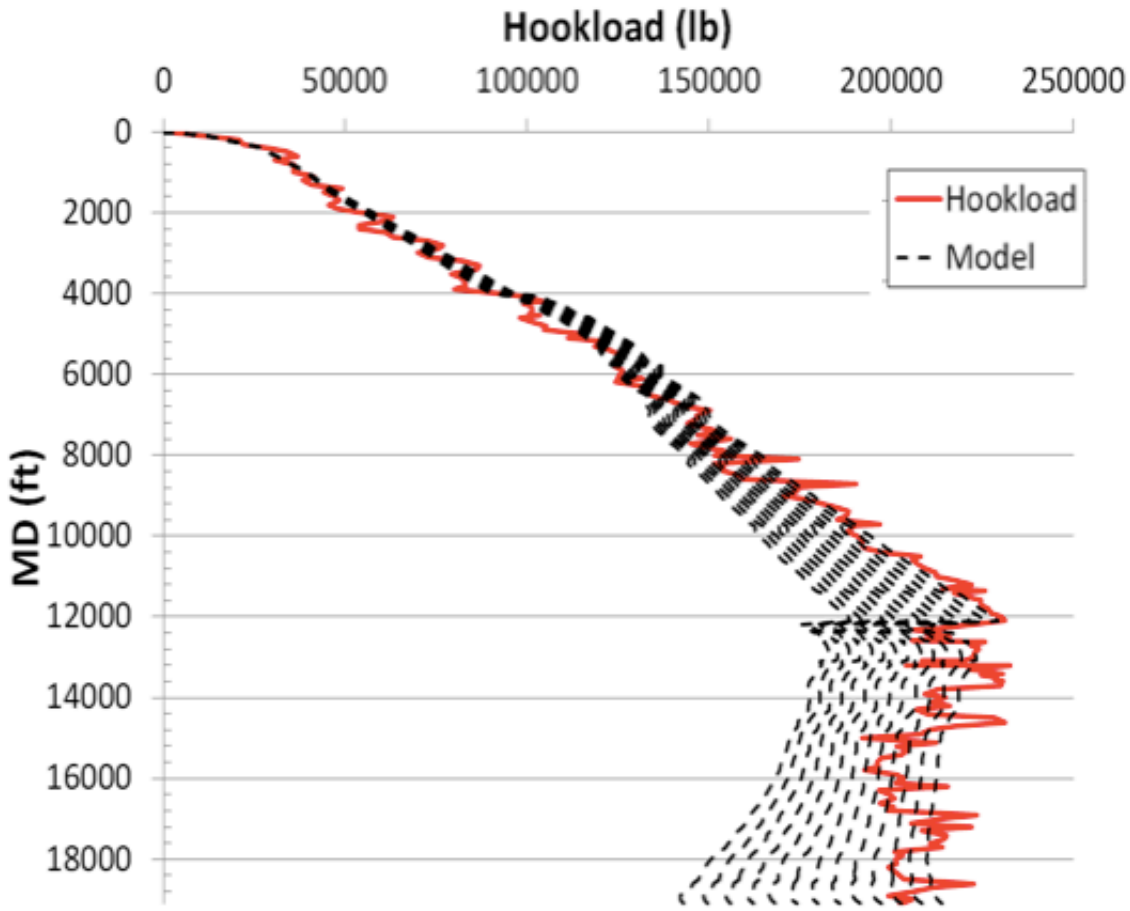

Figure 53: Example of a Broomstick Plot

Each dotted black line represents a different friction parameter, while the solid red line represents the hookload measurements. The most precise friction parameter is found when it is overlapped by the surface measurements. These friction coefficients are averaged over a given span and the result is the most-accurate friction parameter for that span.

REFERENCES

Aadnoy, B., and J. Djurhuus. "Theory and Application of a New Generalized Model for Torque and Drag." SPE 114684. 2008.

Armenta, M. "Identifying Inefficient Drilling Conditions Using Drilling-Specific Energy." SPE 116667. 2008

Banks, S.M., T.W. Hogg, and J.L. Thorogood. "Increasing Extended-Reach Capabilities Through Wellbore Profile Optimization." SPE 23850. 1992.

Brett, J.F., A.D. Beckett, C.A. Holt, and D.L. Smith. "Uses and Limitations of Drillstring Tension and Torque Models for Monitoring Hole Conditions." SPE 16664. 1989.

DuPriest, F.E., and W.L. Koederitz. "Optimizint Drill Rates with Real-Time Surveillance of Mechanical Specific Energy." SPE 92194. 2005.

Ho, H-S. "An Improved Modeling Program for Computing the Torque and Drag in Directional and Deep Wells." SPE 18047. 1988.

Johancsik, C.A., D.B. Friesen, and R. Dawson. "Torque and Drag in Directional Wells—Prediction and Measurement." SPE 11380. 1984.

Johnson, E., J. Land, M. Lee, and R. Robertson. "Landing the Big One—The Art of Fishing." *Oilfield Review*. Winter. 2012/2013.

Kucs, R., H.F. Spörker, G. Thonhauser, and P. Zoellner. "Automated Real-Time Hookload and Torque Monitoring." SPE 112565. 2008.

Lesage, M., I.G. Falconer, and C.J. Wick. "Evaluating Drilling Practice in Deviated Wells with Torque and Weight Data." SPE 16114. 1988.

McCormick, J. and G. Liu. “Torque and Drag Modeling Advanced Techniques and Troubleshooting.” SPE 156945. 2012.

Mitchell, R.F. “Drillstring Solutions Improve the Torque-Drag Model.” SPE 112623. 2008.

Mitchell, R.F. and R. Samuel. “How Good is the Torque/Drag Model?” SPE 105068. 2009.

Mitchell, R.F., A. Bjorset, and G. Grindhaug. “Drillstring Analysis with a Discrete Torque-Drag Model.” SPE 163477. 2013.

Mohan, K., F. Adil, and R. Samuel. “Tracking Drilling Efficiency Using Hydro-Mechanical Specific Energy.” SPE 119421. 2009

Payne, M.L., and F. Abbassian. “Advanced Torque-and-Drag Considerations in Extended-Reach Wells.” SPE 35102. 1997.

Press, W. et al. *Numerical Recipes in Fortran 77*. Cambridge University Press. 1992.

Pessier, R.C., and M.J. Fear. “Quantifying Common Drilling Problems with Mechanical Specific Energy and a Bit-Specific Coefficient of Sliding Friction.” SPE 24584. 1992.

Pessier, R.C., M.J. Fear, and M.R. Wells. “Different Shales Dictate Fundamentally Different Strategies in Hydraulics, Bit Selection, and Operating Practices.” SPE 28322. 1994.

Rae, G.; W.G. Lesso, Jr.; M. Sapijanskas. "Understanding Torque and Drag: Best Practices and Lessons Learnt from the Captain Field's Extended Reach Wells." SPE 91854. 2005.

Rashidi, B. et al. "Real-Time Bit Wear Optimization Using the Intelligent Drilling Advisory System." SPE 136006. 2010.

Sheppard, M.C., C. Wick, and T. Burgess. "Designing Well Paths to Reduce Drag and Torque." SPE 115463. 1987.

Taylor, H.L., and C.M. Mason. "A Systematic Approach to Well Surveying Calculations." SPE 3362. 1972.

Teale, R. "The Concept of Specific Energy in Rock Drilling." *International Journal of Rock Mechanics and Mining Science*. Volume 2, pg 57 – 73. 1965.